

# Neural Co-Processors for Restoring Brain Function: Results from a Cortical Model of Grasping

Matthew J Bryan<sup>1</sup>, Linxing Preston Jiang<sup>1,2,3</sup>, Rajesh P N Rao<sup>1,2,3</sup>

<sup>1</sup> Neural Systems Laboratory, Paul G. Allen School of Computer Science & Engineering, University of Washington, Seattle, WA, USA

<sup>2</sup> Center for Neurotechnology, University of Washington, Seattle, WA, USA

<sup>3</sup> Computational Neuroscience Center, University of Washington, Seattle, WA, USA

E-mail: {mmattb,prestonj,rao}@cs.washington.edu

March 2023

**Abstract.** *Objective* A major challenge in designing closed-loop brain-computer interfaces (BCIs) is finding optimal stimulation patterns as a function of ongoing neural activity for different subjects and different objectives. Traditional approaches, such as those currently used for deep brain stimulation (DBS), have largely followed a manual trial-and-error strategy to search for effective open-loop stimulation parameters, a strategy that is inefficient and does not generalize to closed-loop activity-dependent stimulation. *Approach* To achieve goal-directed closed-loop neurostimulation, we propose the use of brain co-processors, devices which exploit artificial intelligence (AI) to shape neural activity and bridge injured neural circuits for targeted repair and restoration of function. Here we investigate a specific type of co-processor called a “neural co-processor” which uses artificial neural networks (ANNs) and deep learning to learn optimal closed-loop stimulation policies. The co-processor adapts the stimulation policy as the biological circuit itself adapts to the stimulation, achieving a form of brain-device co-adaptation. Here we use simulations to lay the groundwork for future *in vivo* tests of neural co-processors. We leverage a previously published cortical model of grasping, to which we applied various forms of simulated lesions. We used our simulations to develop the critical learning algorithms and study adaptations to non-stationarity in preparation for future *in vivo* tests. *Main results* Our simulations show the ability of a neural co-processor to learn a stimulation policy using a supervised learning approach, and to adapt that policy as the underlying brain and sensors change. Our co-processor successfully co-adapted with the simulated brain to accomplish the reach-and-grasp task after a variety of lesions were applied, achieving recovery towards healthy function in the range 75-90%. *Significance* Our results provide the first proof-of-concept demonstration, using computer simulations, of a neural co-processor for adaptive activity-dependent closed-loop neurostimulation for optimizing a rehabilitation goal after injury. While a significant gap remains between simulations and *in vivo* applications, our results provide insights on how such co-processors may eventually be developed for learning complex adaptive stimulation policies for a variety of neural rehabilitation and neuroprosthetic applications.

*Keywords:* brain-computer interface, brain-machine interface, neurostimulation, neuromodulation, neural co-processor, AI, machine learning, deep learning, neural networks, computational models

## 1. Introduction

Brain-computer interfaces (BCIs) have made significant advances over the last several decades, leading to the control of a wide variety of virtual and physical prostheses through neural signal decoding [1, 2, 3, 4]. Separately, advances in stimulation techniques and modeling have allowed us to probe neural circuit dynamics (e.g. [5]) and learn to better drive neural circuits towards desired target dynamics by encoding and delivering information through stimulation [6, 7, 8, 9, 10, 11, 12, 13]. Bi-directional BCIs (BBCIs) allow stimulation to be conditioned on decoded brain activity and encoded sensor data for applications such as real-time, fine-grained control of neural circuits and prosthetic devices (e.g., [14]).

Motivated by these advances, we investigate here a flexible framework for combining encoding and decoding using “neural co-processors” [15], a type of brain co-processor [16]. Neural co-processors leverage artificial neural networks (ANNs) and deep learning to compute optimal closed-loop stimulation patterns. The approach can be used to not only drive neural activity toward desired activity regimes, but also to achieve task goals external to the subject, such as finding closed-loop stimulation patterns for motor cortical neurons for restoring the ability to reach and grasp an object. Likewise, the framework generalizes to stimulation based on both brain activity and external sensor measurements, e.g., from cameras or light detection and ranging (LIDAR) sensors, in order to restore perception (e.g., cortical visual prosthesis) or incorporate feedback for real-time prosthetic control (see [16] for details).

The co-processor framework also allows co-adaptation with biological circuits in the brain by updating its stimulation policy, while the brain updates its own response to the stimulation via adaptation and neural plasticity, or modifies its response due to other reasons. The co-processor could potentially optimize its outputs for a desired optimization function continually in the presence of significant non-stationarities in the brain.

Here, to lay the groundwork for future *in vivo* tests of the co-processor framework, we use computer simulations to explore how co-processors can be trained to restore lost function and how they can adapt to non-stationarities. We demonstrate a neural co-processor that restores movement in a computational model of cortical networks involved in controlling a limb, after a simulated stroke affects the ability to use that limb. Our demonstration combines both components of a neural co-processor [15]:

- An emulation model based on ANNs, which learns a mapping from stimulation and current neural activity to output variables such as task performance (or future neural activity).
- An artificial intelligence (AI) “agent” based on ANNs which learns the best closed-loop activity-dependent stimulation to apply in real time to optimize a given task.

## 2. Background

Significant advances have been made in understanding and modeling the effects of electrical and other forms of neural stimulation on the brain. Researchers have explored how information can be biomimetically or artificially encoded and delivered via stimulation to neuronal networks in the brain and other regions of the nervous system for auditory [6], visual [7], proprioceptive [8], and tactile [9, 10, 11, 12, 13] perception. Advances have also been made in modeling the effects of stimulation over large scale, multi-region networks, and across time [17]. Some models can additionally adapt to ongoing changes in the brain, including changes due to the stimulation itself [18]. For our simulations described below, we use a stimulation model, not unlike those cited above, which seeks to account for both network dynamics and non-stationarity. In addition to training the model to have a strong ability to predict the effect of stimulation, we additionally adapt it to be useful for learning an optimal stimulation policy, a property distinct from predictive power alone.

Researchers have also explored both open- and closed-loop stimulation protocols for treating a variety of disorders. Open loop stimulation has been effective in treating Parkinson’s Disease (PD) [19], as well as various psychiatric disorders [20, 21, 22]. In research more directly related to our work, Khanna et al. [23] investigated the use of open loop stimulation in restoring dexterity after a lesion in nonhuman primate’s (NHP) motor cortex. The authors demonstrate that the use of low-frequency alternating current, applied epidurally, can improve grasp performance.

While open loop stimulation techniques have yielded clinically useful results, results in many domains have been mixed, such as in visual prostheses [24], and in invoking somatosensory feedback [13]. We believe this is due to the stimulation not being conditioned on the ongoing dynamics of the neural circuit being stimulated. From moment to moment and throughout the day, a neuronal circuit in the brain can be expected to respond differently even when the same stimulation parameters are used, due to the multitude of different external and internal inputs influencing the circuit’s ongoing activity. Stimulation therefore needs to be closed-loop, i.e. proactively adapted in response. This need is even greater over longer time scales as the effects of plasticity, changes in clinical conditions, and ageing change the dynamics and connectivity of the brain. Closed-loop stimulation may also provide means to better regulate the energy use of an implanted stimulator, allowing it to intelligently regulate when to apply stimulation, in order to preserve implant battery life [25]. Another benefit is that closed-loop stimulation offers an opportunity to minimize the side-effects of stimulation, through real time regulation of the stimulation parameters, such as in the use of deep brain stimulation (DBS) in PD patients [26]. In recent years, closed-loop stimulation has been used to aid in learning new memories after some impairment [27, 28], to replay visually-invoked activations [18], and for optogenetic control of a thalamocortical circuit [29], among others.

A major open question is: how does one leverage closed-loop stimulation for real-time

co-adaptation with the brain to accomplish an external task such as restoration of a lost function? “Co-adaptation” here refers to the ability of a BCI to adapt its stimulation regime to ongoing changes in neural circuits in the brain, and to adapt with the brain to accomplish the external task (e.g., grasping). The neural co-processor we present here provides one potential approach to accomplishing this goal. Through the use of deep learning, a neural co-processor co-adapts its AI, which controls stimulation, in synch with the biological circuits in the brain.

For a neurologically complex task such as grasping, it is unlikely that there exists a fixed real-time controller which can be identified *a priori* for stimulating the (potentially impaired) neural circuits involved in the task. This is due in large part to the variability in the placement and performance of sensors and stimulators in different brains, as well as variability in brain structure and function between subjects. The most plausible path to implementing a real-time controller is therefore to allow the device to adapt to the subject, and to the long-term changes in their brain activities, and variability in the sensors, stimulators and hardware. Our proposed neural co-processors seek to accomplish such adaptation through ANNs and deep learning, and a particular training paradigm described below.

### 2.1. Simulation as a Way to Gain Insights Prior to *in vivo* Experiments

To gain insights into neural co-processors before testing them *in vivo*, we investigated a number of crucial design elements through the use of a previously published model by Michaels et al. [30] of the cortical areas involved in grasping; the model, based on multiple recurrent neural networks, is inspired by cortical anatomy and was fit to data from nonhuman primates performing grasping tasks. Using this cortical model as a “simulated brain” allowed us to rapidly iterate through different design and training methods to demonstrate key properties of the neural co-processor framework. These insights will help guide the co-processor training methodologies and experimental design for future *in vivo* experiments. Additionally, a commonly-accepted maxim of animal experimentation is that animal use should be narrowly tailored to answering questions which cannot be answered in other ways. Consider, for example, “the 3Rs alternatives” approach to the use of animal experiments [31]. In our case, we leverage computer simulations for initial investigations into co-processor design, gathering evidence in preparation for future *in vivo* experiments. In the Discussion section, we explore potential paths for translation of this work to *in vivo* experiments.

A previous example of such a simulation approach is the work of Dura-Bernal et al. [32]. In this work, the authors used a simulated spiking neural network to train a stimulation agent. Their stimulation agent sought to restore the network’s control of a simulated arm to reach a target, after a simulated lesion was applied. Similar to our approach, the authors simulated lesions by effectively removing parts of their simulated network, or by removing connections between parts of the network. As the authors point out, there exists only limited ability to probe a neural circuit *in vivo* in

order to perform learning. As a result, we first need to design our approach through the use of an admissible simulation. The key question then is: how can we design an admissible simulation, i.e. one which provides a test bed on which we can demonstrate key properties of our co-processor designs? We answer this question in our work by adopting a previously published model of cortical grasping [30] that has been shown to replicate properties of the cortical circuit in the biological brain based on fits to nonhuman primate data.

Through our simulation, we explored what properties of the co-processor allow successful adaptation to the short-term dynamics of the cortical model as it is being stimulated, as well as adaptation to longer-term connectivity changes in the cortical model. We present a training method for neural co-processors for learning optimal stimulation patterns that drive improvements in external task performance, while also adapting to the non-stationarity of the stimulated neural circuits.

### 3. Methods

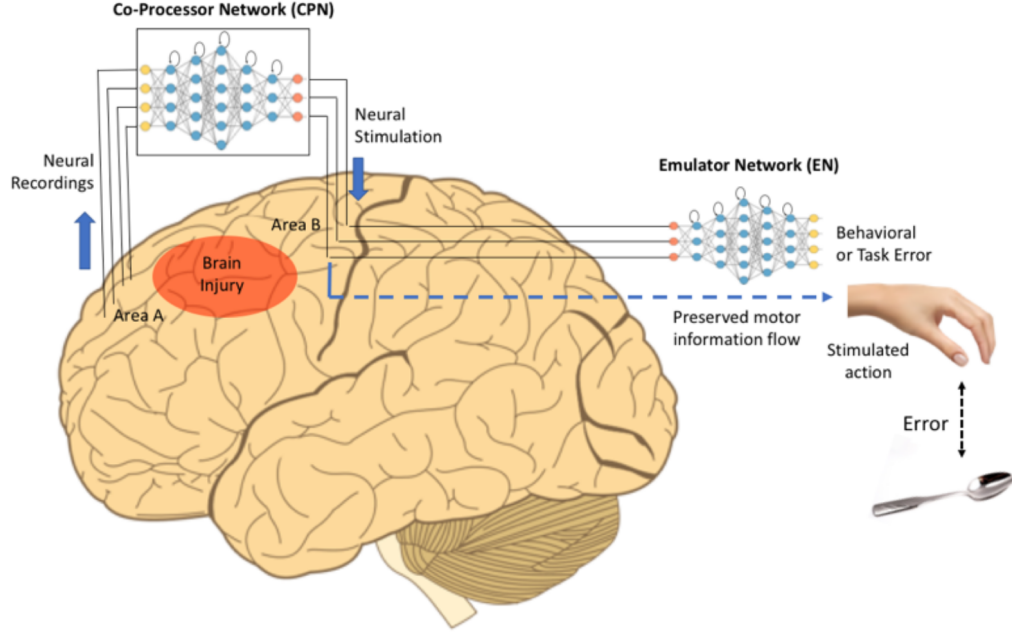
#### 3.1. Architecture Overview

First, we present the architecture of our neural co-processor design. This design aims to solve two fundamental challenges in using neural stimulation to improve external task performance. First, to restore function for complex tasks (such as grasping), it is difficult to determine the mapping between observed neural activity and the stimulation patterns to be applied to a downstream motor area. As a result, the co-processor must learn what stimulation pattern is appropriate for achieving the external task given the current neural activity. Unfortunately, in most cases, we do not know what the correct stimulation pattern is for any given input activity pattern, a precondition for using supervised deep learning methods for training the co-processor. Stimulation shapes the nonlinear dynamics of circuits in the brain in complex ways, leading to complex effects in external behavior. It is therefore not obvious what stimulation patterns will produce a desired behavior.

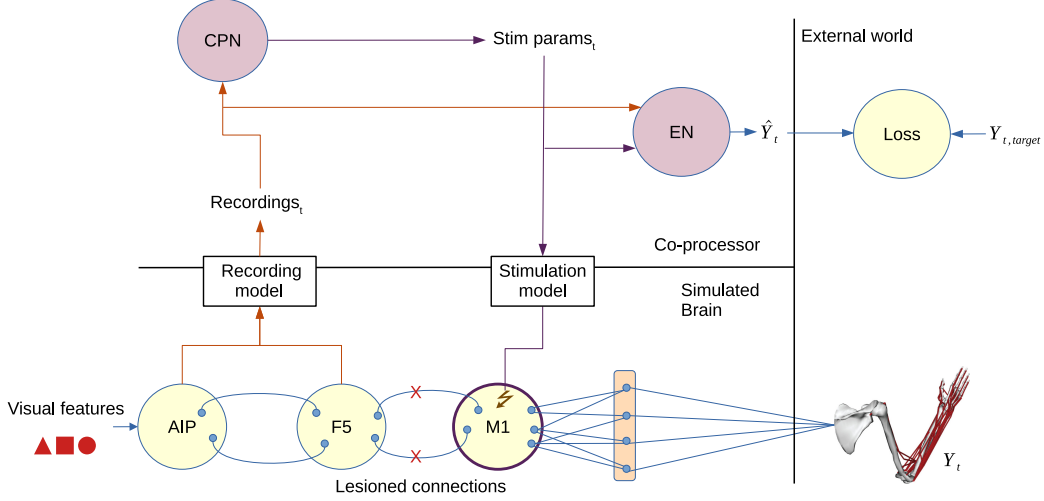
A neural co-processor attempts to solve these problems with a pair of artificial neural networks (Fig. 1):

- a “Co-Processor Network” (CPN), which is a recurrent neural network (RNN) which maps neural activity, and possibly data from external sensors, to appropriate stimulation parameters.
- an “Emulator Network” (EN), also an RNN which models the effect of stimulation on neural dynamics and behavior for the external task.

The CPN can be trained using the backpropagation algorithm, the workhorse of deep learning for training ANNs. However, backpropagation requires the error between the output of the CPN and a desired output, and as discussed above, we do not have the desired output stimulation pattern. We do however know what the desired output behavior in a task should be, e.g., a particular kind of grasp for a particular object or a



(a)



(b)

Figure 1: **Neural co-processor for restoring function after a brain injury.** An artificial neural network called the “Co-Processor Network” (CPN) is used to map input neural activity patterns in an area A to output stimulation patterns in same or other areas B in order to achieve a neural or behavioral goal using another ANN, an “Emulator Network” (EN) - see text for details. (a) The example here shows the CPN creating a new information processing pathway between prefrontal cortex and motor cortex, bypassing an intermediate area affected by brain injury (e.g., stroke). Adapted from [15], (b) Our current study involves a simulated cortical grasping circuit. The CPN and EN both receive simulated brain recordings, which are created according to a recording model (see Methods). The CPN outputs stimulation parameters, which are applied to the simulated grasping circuit, according to a stimulation model. The EN models the relationship between the stimulation, brain recordings, and external task.

particular type of neural activity in a brain area corresponding to healthy activity. We can therefore compute the error between this desired behavior and the actual behavior caused by the CPN due to stimulation. How do we backpropagate this external task error to update the parameters of the CPN so that it learns to produce stimulation patterns that are optimal for the task?

We use a trained EN to backpropagate the external task error to the CPN, which then uses this backpropagated error to update its parameters. We train the EN to predict task-relevant parameters - a prediction of muscle velocities in our case - given randomly sampled stimulation patterns or stimulation patterns output by the CPN, and any measured neural activity. If the EN is trained to a sufficiently high level of precision, it can be used as a function approximator for the subject’s true “stimulation function”. When training the CPN, we treat the EN’s output as the actual task output (e.g., actual grasp behavior or muscle velocities). We backpropagate through the EN (without changing its parameters) and then the CPN (changing its parameters) the error between the EN’s output and the desired task output (see Fig. 1).

In our experiments, the EN was a single-layer fully-connected long short-term memory (LSTM) recurrent neural network, with hyperbolic tangent (*tanh*) activations, and a linear readout. It had 87 LSTM neurons, the number being chosen somewhat arbitrarily as a function of the input and output vector sizes. We found that varying this neuron count did not drastically change results. Although other architectures could also be used, we found that this LSTM architecture allows the EN to continuously adapt to long-running dependencies in the simulated neural dynamics, far better than a vanilla RNN. The CPN had an almost identical architecture, but with 61 LSTM neurons. As with the CPN, this neuron count was chosen as a function of the input and output vector sizes, and increasing it had little effect on results. There is no requirement for the EN and CPN to have similar network architectures, but we found that these choices worked well in our experiments.

Note that the EN is more general than traditional models of neurostimulation which attempt to predict the effects of stimulation on *neural activity*. The EN in a neural co-processor predicts the effects of stimulation (taking into account ongoing neural dynamics) on *task performance*. This provides the key functionality needed to train the CPN. In the special case where the task involves driving neural circuits in the brain to desired neural activities, the EN reduces to more traditional models of stimulation.

For comparison, consider an EN architecture based on a traditional RNN with a nonlinearity. This is a nonlinear version of the common linear time-invariant state space stimulation model studied in previous research (see, e.g., [17]). We found, however, that compared to an LSTM-based EN, the linear model and the vanilla nonlinear RNN are both not sufficiently powerful to capture the long-term dependencies in stimulation effects needed for the CPN to learn well. Our use of an LSTM for learning an EN builds on previous work using LSTMs for predicting the evolution of local field potentials [33] and blood-oxygen-level dependent (BOLD) hemodynamic responses [34] over time.



### 3.2. Simulation Overview

To test the feasibility of the neural co-processor approach, we used a previously published cortical model for grasping in a nonhuman primate (NHP) brain. Using such a model allowed us to explore some of the critical architectural choices and training algorithms for neural co-processors, enabling us to rapidly and cheaply iterate on our design, laying the groundwork for future *in vivo* experiments.

Specifically, we use the cortical model of Michaels et al. [30] (Fig. 2a). The model, which uses multiple RNNs to represent multiple interconnected cortical areas, was trained to mimic the grasping circuits of NHP subjects engaged in a delayed reach-to-grasp task. The model’s design draws on a body of literature focused on architectures and training methods for RNNs which seek to create artificial neural networks with activation dynamics similar to biological circuits, including circuits for delayed grasping tasks [35]. The model consists of three “modular” vanilla RNNs (mRNNs), representing the cortical areas AIP (anterior intraparietal cortex), F5 (ventral premotor cortex) and M1 (primary motor cortex) respectively, and a linear readout layer from M1 producing muscle velocities (Fig. 2a). Each “module” consists of 100 vanilla RNN neurons, with a nonlinearity applied on the outputs. The modules are internally fully connected, and are connected to each other sparsely (10% connectivity in our case). The inputs to the network are visual features representing the object to be grasped, as well as a hold signal. The visual features intend to capture the features represented in the subject’s visual cortex. They were extracted using VGGNet [36] from 3D renderings of the same objects which the subjects grasped. The hold signal is a Boolean which encodes the point in the experiment when the subject began to reach. The outputs of the network are muscle velocities for the shoulder, arm, and hand of the subject. The actual velocities were captured with a motion capture glove. The Michaels et al. network model was trained to recapitulate these grasping motions.‡

The Michaels et al. cortical model implements a vision-to-grasp pipeline, from the visual processing needed to move the hand to the appropriate position to shaping the hand for grasping an object of a particular shape. The emergent dynamics of the model’s modules, once trained, correspond roughly to neural responses in the cortical areas AIP, F5, and M1 in a NHP subject’s brain (Fig. 2a; see [30] for details). For convenience, we will refer to the three modules in the model using the cortical areas (AIP, F5, M1) they correspond to. For details on how this network model was trained, please see Supplementary Materials 7.2. For additional details on the task structure, see Supplementary Materials 7.1.

An important attribute of this cortical model is that the simulated circuit’s activity shows a relatively clear separation for different object shapes, i.e., the visual input is leveraged by the model to successfully generate hand shape trajectories for grasping

‡ Data and trained models from this work were supplied to us by the lead author of [30]. We re-implemented their model in PyTorch, and used their trained parameters for an arbitrarily chosen subject.

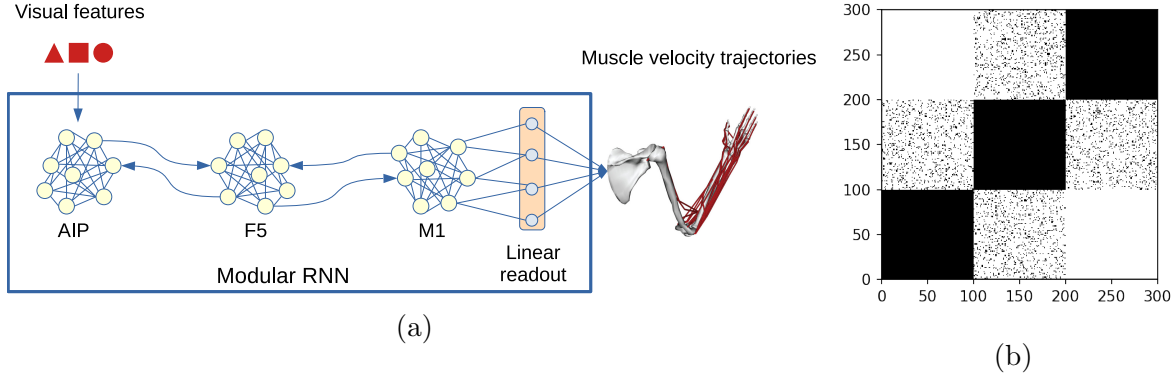


Figure 2: **Architecture of the Cortical Model for Grasping.** (a) Modular RNN (mRNN) used by Michaels et al. [30] to model cortical circuits involved in grasping objects. The emergent dynamics of the three modules correspond well to neural activity in primate cortical areas AIP, F5, M1, respectively, for the same task. Visual features of an object (derived from VGGNet) propagate forward through the network, conditioning the grasp on the object’s size and shape. (b) Connectivity matrix  $J$ . Connected neuron pairs are indicated in black, though the actual network weights are floating point values. White indicates non-connections. Note the each module is fully connected (black squares along the diagonal) while connections to adjacent modules are sparse (10% of possible connections). All connections were trained using nonhuman primate (NHP) data to recapitulate the experimentally recorded muscle velocity trajectories for grasping different objects.

objects of particular shapes and sizes. As noted below, if this visual information is prevented from propagating through the cortical modules (e.g., due to a simulated lesion), the model can at best learn a stereotyped grasp across all object sizes and shapes.

*3.2.1. Lesioning the cortical model causes real world failure modes* As shown by Michaels et al. [30], simulated lesions in the cortical model described above result in error modes which resemble the effects of some natural lesions in the primate brain. For example, a “lesion” involving zeroing some of the outputs of the first (AIP) module leads to a reaching motion generally succeeding, but finger muscle velocities show a higher degree of error, effectively implying that the subject can reach to grasp, but cannot tailor the grasp to the current object. This is likely due to object shape information not being fully conveyed to the primary motor cortex (M1) module. Such a form of hand muscle spasticity is also a common symptom in certain strokes where the subject is able to position their hand, but is unable to form the appropriate grasp [23, 37].

On the other hand, if we lesion a portion of the M1 module in the model, we see a more complete loss of movement, affecting even the ability to reach for the grasp. Finally, if we “disconnect” communication between the F5 and M1 modules, we see a failure similar to an AIP lesion: the reaching movement is generally achieved, but

we see a disproportionate impact on forming the appropriate hand grasp. See Fig. 3a for examples of lesion impacts on velocities for individual muscles. In Fig. 3b we see the ratio of mean squared error (MSE) loss for hand muscles to all muscles. Values greater than 1.0 indicate that hand muscles are impacted more than other muscles. Note that with the AIP and connection lesions, hand muscles show significantly higher loss than overall loss. However, the M1 lesion shows the highest overall loss; see Table 3 in Supplement materials section 7.9 for detailed lesion loss data.

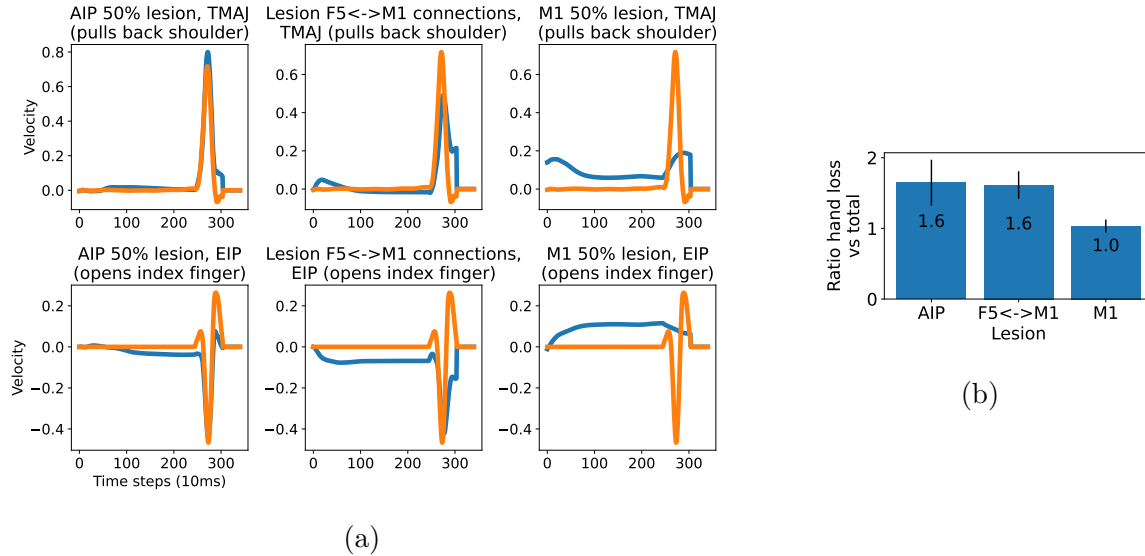


**Figure 3: Simulating strokes by lesioning different parts of the model lead to differential impact on grasping behavior.** (a) Example muscle trajectories before (orange) and after (blue) simulated stroke due to AIP, F5-M1 and M1 lesions for a shoulder muscle (top row) and a hand muscle (bottom row). Lesions which prevent a forward propagation of visual information tend to have a larger effect on hand pose (example EIP muscle shown) than on the shoulder, which is more involved in the reach motion (example TMAJ muscle shown). Lesions of M1 tend to cause a significant task loss on both. (b) Ratio of hand muscle mean squared error (MSE) losses vs. overall MSE losses, for different lesion types. The loss is measured relative to the model’s movement trajectories prior to the lesion. Average of all trials, with  $\pm 1$  stdev shown. Higher ratios for AIP and connection lesions indicate those lesions cause a larger loss for hand movement than overall movement, though their overall loss is lower than for M1 (see Table 3).

Given a particular type of lesion in the model, the goal of the co-processor is to learn to map “neural recordings” (derived from current mRNN activity in the model) to the appropriate stimulation pattern for executing the required grasp. The co-processor thus seeks to effectively bridge across the lesion and deliver stimulation to enable grasping behavior tailored to the current object’s shape.

In our experiments, we studied our co-processor’s performance on three types of

simulated lesions:

- **Loss of AIP Neurons:** We force the output of some proportion of the AIP module’s neurons to zero, effectively removing them from the network. This results in some amount of loss of object shape information.
- **Loss of F5-M1 Connections:** We prevent the propagation of information between the F5 and M1 modules, effectively representing a severing of the connections between the two modules. Note that the connections are sparse and run in both directions, and we lesion the connections in both directions.
- **Loss of M1 Neurons:** We force the output of some proportion of the M1 module’s neurons to zero. Here, the lesion may make it impossible for the co-processor to find a perfect solution since the loss of M1 neurons may make it impossible to activate muscles in the same ways as before the lesion. However, in the Results section, we show that some recovery is still possible.

*3.2.2. Simulated network exhibits long running and stable dynamics* To compute stimulation patterns that optimize for a task, the co-processor must learn to adapt to the dynamics of the network it is stimulating. Biological neural networks as well as our simulated grasping network exhibit long range changes in dynamics due to stimulation. A perturbation of the network (i.e., due to stimulation) will cause changes in neuronal activations long after the stimulation has been applied, sometimes far from the site of stimulation. Our cortical grasping network model exhibits the same behavior.

To illustrate this, suppose we apply a small, one-time perturbation to the hidden states of 10 randomly chosen neurons in the output (M1) module at some point in time during a trial. By repeating this experiment many times, we can understand what the distribution of long-running effects tends to look like on the output muscle velocities.

In Fig. 4 we see that even a single, one-time perturbation in the network has effects dozens of time steps later. Our co-processor will need to learn to take these dynamics into account. As we will show in the next subsection, the problem our co-processor faces in our simulations is in fact even harder than this since we also incorporate a model of stimulation effects on the neural circuit which includes both spatial and temporal smoothing.

*3.2.3. Stimulation model* In our experiments, we stimulate neurons only in the output area (here M1) since the co-processor’s purpose is to improve external task performance, which it is able to do with appropriate stimulation of the M1 output region of the network model. In a more general setting, it is conceivable that a co-processor could stimulate other areas of the brain as well to improve task performance downstream, or to probe the brain to better reveal the user’s intent (i.e. object shape), but we leave these directions to future work.

To make our stimulation model more realistic, rather than allowing stimulation to directly change the output of single neurons, we simulated how stimulation may affect a

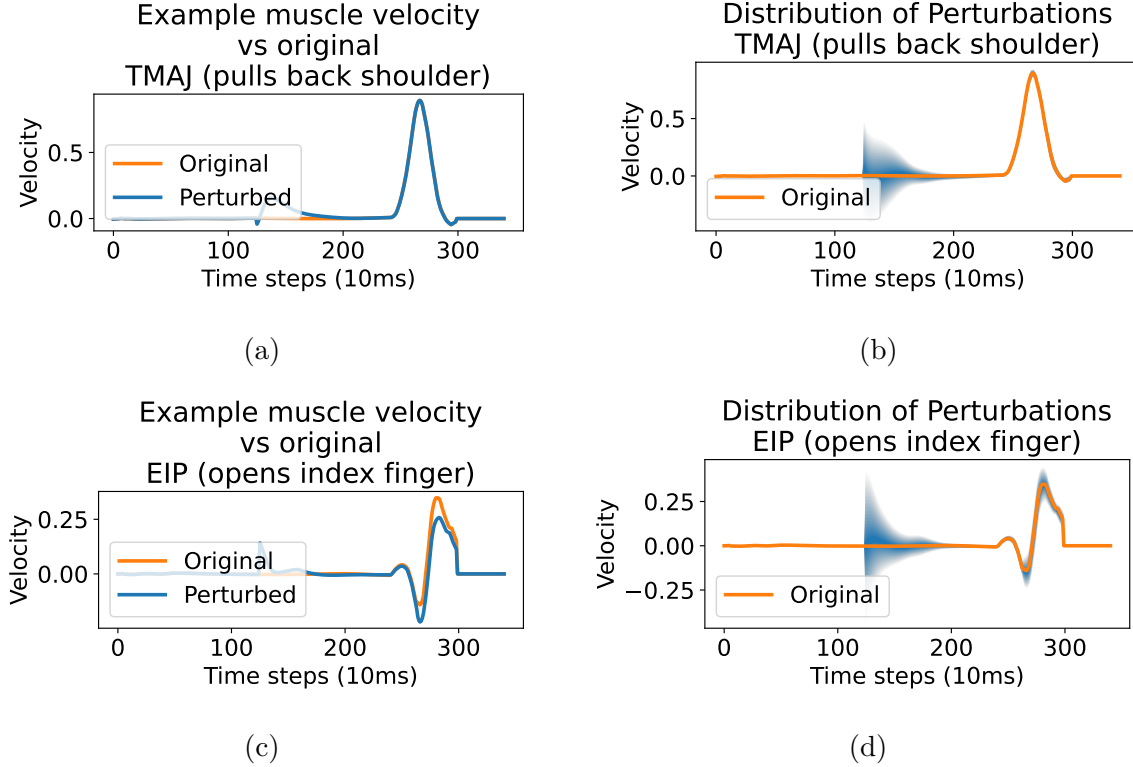


Figure 4: **Perturbations of the simulated cortical network (i.e. due to stimulation) have long-running effects on muscle activation.** Our results are consistent with the fixed point analysis of the network in [30], showing that the network exhibits stability. It tends towards the original trajectory after perturbation. Instantaneous random perturbation of a random group of 10 M1 neurons performed at time  $t=2s$ . (a, c) Single trial example for TMAJ, EIP muscles respectively. (b, d) Distribution of effects across  $n=1000$  samples on TMAJ, EIP muscles respectively. Probability distribution shown to  $\pm 2$  stdevs. Network exhibits similar behavior when perturbation is applied at other time steps.

network of neurons using a model that incorporates aspects of both spatial and temporal smoothing. Our intent was not to create a biophysical model of stimulation (our model does not arrange neurons in a volume to allow for such detailed simulation). Instead, the stimulation model approximates the effects of *in vivo* biological stimulation (e.g., extracellular electrical stimulation) by diffusing the effects of stimulation across many neurons and across time. Our EN must thus learn to approximate this stimulation model, in addition to approximating the cortical dynamics of the brain and the mapping of those dynamics onto the grasping outputs. §

Our stimulation model uses a function which receives as input the stimulation parameter vector  $\theta$  from the CPN. The function performs temporal smoothing using a simple exponential decay model by adding its current input to an exponentially decaying

§ In Supplementary Materials section 7.5, we explore other stimulation models.

sum of inputs that decays towards 0.0 at some rate (see Equation 1 below). The effect of stimulation is thus not instantaneous, but rather decays with time. Likewise, to simulate the difficulty of stimulating only single neurons, we applied Gaussian smoothing to map  $\theta$  (16-D in our experiments) to changes in the activations of a large number of the simulated M1 neurons (100 neurons in our experiments). If we assume each element of the  $\theta$  represents the stimulation parameter for a single electrode, our Gaussian smoothing operation emulates how stimulation may affect the neurons in its vicinity more than it affects neurons further away. To accomplish this, we assume our model neurons are aligned along a spatial dimension arbitrarily and fix  $\sigma = 1.75$ .

The resulting equations which define our stimulation model are:

$$\alpha_t = \tau\alpha_{t-1} + \theta_{t-1} \quad (1)$$

$$s_t = C\alpha_t \quad (2)$$

- $\alpha$ : the 16 dimensional internal state of the stimulation function
- $\tau$ : our decay rate for temporal smoothing, which we set arbitrarily to 0.7
- $C$ : a fixed  $100 \times 16$  Gaussian smoothing matrix containing a single 1-D Gaussian in each column, to implement spatial smoothing and spread of stimulation to the stimulated neural population.
- $s_t$ : the spatiotemporally smoothed stimulation vector whose elements denote how much stimulation is applied to each neuron at time step  $t$  (see Equation 3 below).

The governing equations of an mRNN with stimulation then become:

$$x_{t+1} = Jx_t + Iv_t + s_t + b \quad (3)$$

$$a_t = \tanh(x_t) \quad (4)$$

$$y_t = La_t + l \quad (5)$$

- $x$ : the hidden state of each model neuron
- $J$ : recurrent weight matrix
- $I$ : input weight matrix
- $v_t$ : input
- $b$ : activation bias
- $L, l$ : parameters of the linear readout layer
- $y_t$ : the output of the network

Fig. 5 depicts an example where  $\theta$  is non-zero at  $t = 0$  and zero for all other times, illustrating the effects of stimulation on the network across space and time. Fig. 6 illustrates the effects of stimulation during a stroke simulation. In this case, the trial is one where 50% of M1 neurons have been lesioned (their outputs are zero), the inputs to the CPN are from the AIP and F5 modules, and stimulation is applied to the M1 module.

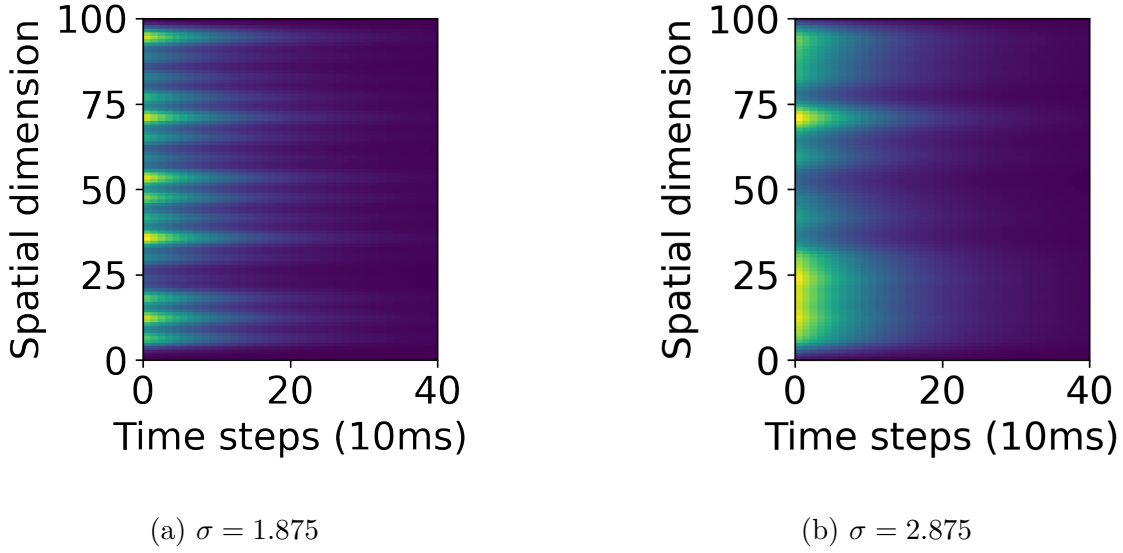


Figure 5: **Simulating the effects of stimulation on a recurrent network across space and time.** The stimulation model performs spatial and temporal smoothing of a 16-dimensional vector of stimulation parameters  $\theta$  onto 100 neurons in a recurrent network. The 16 elements of the vector represent in-effect 16 electrodes located evenly along a spatial dimension, along which the 100 neurons are arranged arbitrarily. We show here the effects of two randomized  $\theta$  with two respective smoothing parameters  $\sigma$  (a.  $\sigma = 1.875$ , b.  $\sigma = 2.875$ ). After  $t = 0$ ,  $\theta$  is the zero vector. Color values indicate the magnitude of the value summed into each neuron’s hidden state at that time step.

*3.2.4. Recording model* To simulate recordings of our model neurons, we used a recording model that assumed that the model neurons are laid out along a single spatial dimension with a given number of electrodes spread evenly apart. We then applied Gaussian convolution, where the Gaussian kernel is centered at each electrode position. Thus, the recording from each “electrode” is a Gaussian-weighted average of the activities of all model neurons in the given module. Fig. 6 (bottom right panel) shows an example of recordings obtained using this recording model; note that the Gaussian averaging provides a potentially ambiguous view of the activities of the underlying neurons due to the inherently destructive nature of averaging, making it more challenging for the co-processor to interpret the neural activity and produce an appropriate stimulation pattern. Our simulated recordings are similar in spirit, though not actually modeling, local field potentials (LFPs) recorded extracellularly in biological neural tissue. In Supplementary Materials section 7.6, we show that as we vary the observability of our “simulated brain” via this recording model, the results remain largely the same, up to the point where the objects to be grasped can no longer be distinguished from the neural recordings due to excessive averaging.

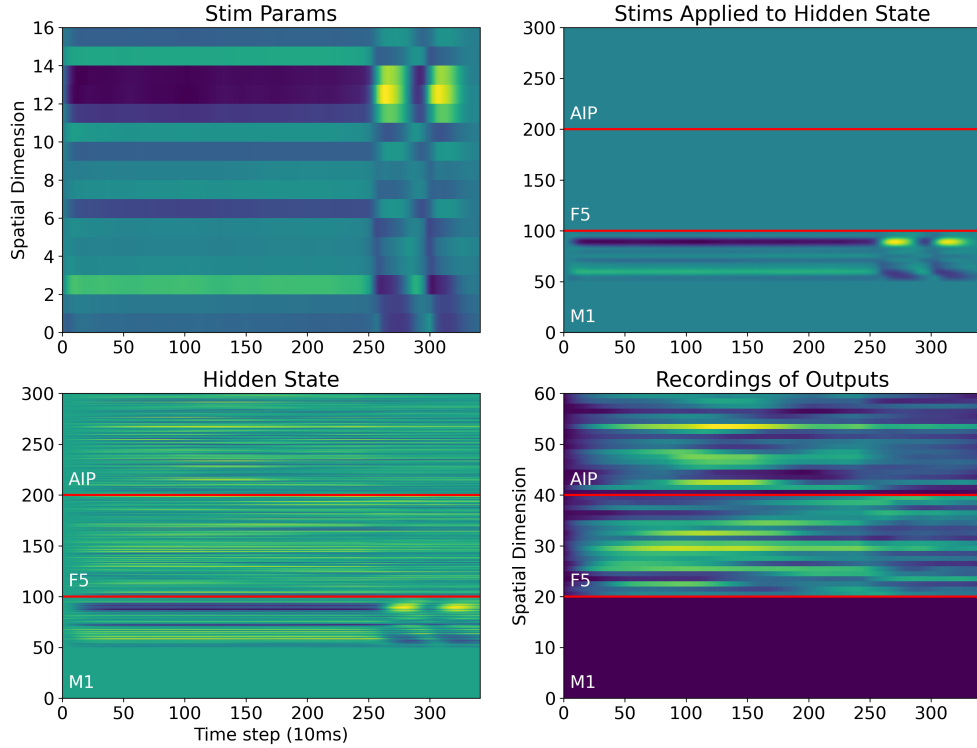


Figure 6: **Example of stimulation and recording for a single trial.** Here, M1 has been lesioned 50%, indicated by hidden states of M1 neurons with a value of zero (bottom left panel, lowest part of the plot). We record neural activities (using the recording model) from only the AIP and F5 modules, as explained in Section 3.4. Stimulation is applied to M1 to drive the network’s output. Stimulation is mostly constant until approximately  $t=250$ , when the hold signal was lifted and the reach began.

*3.2.5. Simulating co-adaptation by the brain* To demonstrate the co-processor’s ability to co-adapt with the brain as it adapts to the co-processor’s stimulation, we modify the cortical grasping network model’s parameters (synaptic weights and biases) throughout the co-processor’s training. We use the standard error backpropagation algorithm to adapt the grasping network to minimize task loss for the object grasping task (using *PyTorch*’s implementation of the *AdamW* optimizer). With each trial, task loss is calculated based on the NHP training data and backpropagated through the mRNNs as they receive stimulation. The learning rate was set arbitrarily to a relatively low rate of  $1e-7$  so that the network adapts more slowly than the co-processor.

*3.2.6. Simulating recovery prior to co-processor use* After a stroke, the human brain has the ability to learn and recover to some extent the behaviors affected by the stroke. We simulated this ability in our grasping network model by re-training the network for



the grasping task after lesioning it. For our simulated lesions which zero-out the outputs of neurons, we found that the cortical model has sufficient redundancy built into it that lesioning it by inactivating large numbers of neurons often leaves enough remaining degrees of freedom that a nearly full recovery can occur. We therefore explored lesions of the model (specifically lesions of AIP and M1 modules) under two conditions: (a) No co-adaptation: the cortical model was not re-trained after the lesion, allowing us to study how much of lost function the co-processor can learn to restore on its own, and (b) Co-adaptation: the cortical model was re-trained after the lesion, allowing us to study how the co-processor copes with non-stationarity as our simulated brain recovers from its lesion.

In the case of a lesion that prevents communication between the F5 and M1 modules, information about the input object’s shape cannot propagate forward in the network to allow shaping of the hand for grasping. However, the cortical model can learn a stereotyped grasp during the recovery period. After this recovery period, a co-processor can help further boost grasp accuracy by forward-propagating object shape information from AIP and F5 to M1, acting as an artificial neural bridge. We explore this application of the co-processor in one of our experiments below.

*3.2.7. Simulating a non-stationary recording function, e.g., sensor drift* Over time, implanted sensors may drift from true readings. We explored the co-processor’s ability to adapt to non-stationarity in the recording function. We performed an experiment where the recording function includes an added bias term which changes over time, according to a random process. Each epoch, we add a random value to each element of the bias term, drawn from a zero-mean Gaussian distribution, causing the “recordings” to drift over time. See Supplementary Materials section 7.4 for further details.

### *3.3. Training Paradigm*

To train the CPN to generate appropriate stimulation patterns for grasping a given input object of a particular shape, we would like to use a learning algorithm such as the backpropagation algorithm and minimize the errors between the current generated grasp (in terms of muscle velocities) and the desired target grasp. However, backpropagation requires the error to be in terms of CPN output stimulation error. We cannot backpropagate grasp error through biological networks in the brain to get the error needed to train the CPN. This motivates our use of the EN as a model for the transformation from stimulation to muscle velocities: we backpropagate grasp error through the EN, while keeping its parameters fixed, and use this backpropagated error to change the parameters of the CPN in order to minimize grasp error.

Using the EN to train the CPN requires careful interleaving of EN and CPN training epochs. EN training epochs concentrate on updating the EN, based on observations of the effect of stimulation on the cortical network model’s output. The loss function when training the EN is the mean squared error (MSE) loss between the EN’s prediction

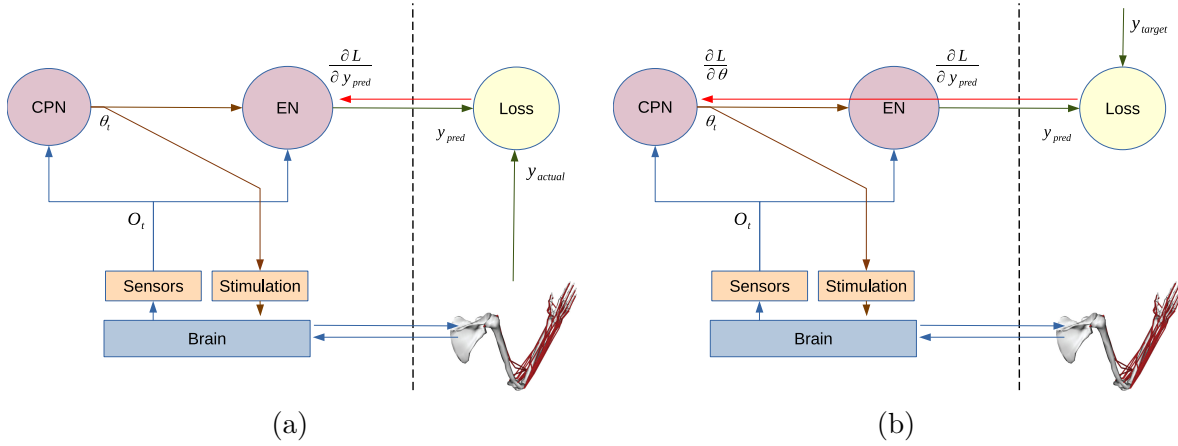


Figure 7: **Training the neural co-processor.** (a) EN training phase: backpropagate the error between actual vs predicted muscle velocities through the EN to update the EN’s parameters. (b) CPN training phase: backpropagate the error between EN’s predicted output vs target muscle velocities, via the EN (without changing its parameters) and through the CPN, to update the CPN’s parameters. Note that we are effectively treating the EN’s predicted output as the actual muscle velocity output, and therefore it is important to have a good pre-trained EN.

and the actual output of the cortical model (i.e., muscle velocities). During the CPN training epochs, we keep the EN’s parameters fixed and use the EN to train the CPN. Specifically, we backpropagate the MSE loss between the EN’s predicted output, and the desired output (target muscle velocities for grasping the input object) through the CPN. Fig. 7 illustrates the EN and CPN training processes.

*3.3.1. Training and testing data sets* For training and evaluation of our model, we use the same data as in Michaels et al. [30]. The data consist of:

- The input visual features and hold signal. We input these to the simulated cortical model;
- The object identity. We use this to calculate how well the co-processor can differentiate objects; see Results section below;
- The muscle velocity data for the trial, as extracted from the data glove of a nonhuman primate during the NHP trial, and as processed by Michaels et al. [30]. This is our target output.

For each training session, we hold out a random sample of 20% of the data to act as our validation data set; we use the other 80% for training.

*3.3.2. EN training* For the EN to be useful for training the CPN, it must accurately predict the behavioral effects of stimulation produced by the CPN. In addition, backpropagating through the EN must yield gradients which are useful for changing

the weights of the CPN in order to produce better stimulation patterns for minimizing the error. We discovered that this latter property does not occur simply by virtue of the former. Specifically, an EN can be trained to high levels of predictive power, even for random stimulation, and to orders of magnitude lower loss than the task loss, while at the same time, backpropagation through the EN still yields gradients which lead to unstable training of the CPN.

We hypothesize that the crux of the EN training problem is one of over-fitting: the EN may be trained to achieve high predictive power on a data set of stimulation examples, but due to the high dimensionality of our stimulation parameters  $\theta$ , and the dynamics of the network being stimulated, the function learned by the EN may not provide gradients suitable for the stimulation inputs generated by the CPN during its training.

To address this problem, we first structure the training dataset for each EN training epoch in a specific way. In each epoch, we include:

- training examples using stimulation inputs generated by the current CPN;
- training examples using stimulation inputs generated by a small collection of CPNs obtained by adding zero-mean Gaussian noise to the current CPN’s parameters; and
- training examples with white noise stimulation inputs.

Such a training paradigm is designed to cover a sufficient variety of examples to prevent overfitting, and to do so in a way that explores the neighborhood of the current CPN’s parameter space. Augmenting a CPN-generated data set with white noise examples alone was not sufficient to stabilize CPN training, but including additional examples generated by CPNs in the neighborhood of the current CPN helped train the EN to perform well in that neighborhood and produce useful gradients for the CPN. “Neighborhood” here refers to the region of CPN parameter space near the current CPN. This may cause the EN to be overfit, i.e., fit to the local area of CPN parameter space but exhibiting poor predictive power in other areas of the space. However, we solve this problem by retraining the EN, interleaved with CPN training. We show the effect of this paradigm in our results below (section 4.3).

We composed each batch of EN training data as follows:

Source	Proportion of dataset
Data from current CPN	10%
Data from current CPN with parameter noise	60%
Data from white noise stimulation	30%

Additionally, we use decoupled weight decay regularization [38] to mitigate overfitting, and a carefully chosen learning rate schedule. The schedule begins with a higher learning rate initially ( $4e-3$ ), ramping down to a lower rate ( $1e-4$ ). The learning schedule is based on the most recent prediction error on the validation portion of the data set. We found that using rates much lower or higher than these rates in any training phase may cause the EN learning to not converge. EN training proceeds

until the network’s prediction error is lower than a threshold, defined as a fraction of the current CPN’s task loss. Section 3.3.4 provides further details on when we switch between training the EN and CPN.

*3.3.3. CPN training* Once an EN is properly trained, we can use the EN as a surrogate for the cortical model’s transformation of stimulation patterns and neural activity to grasping behavior (i.e., muscle velocities). We use a large number of randomly sampled trials from the original Michaels et al. task [30] and generate stimulation patterns using the current CPN alone. These stimulation patterns are passed through the EN to generate predictions of output muscle velocities, which are compared to the desired target velocities to compute the error. We backpropagate this error through the EN (without modifying its parameters) to generate training gradients for the CPN. Fig. 7 illustrates this training process.

We found that the CPN appears to train in two phases. In the first phase, it is largely learning the structure of the reach-to-grasp task, e.g., that the muscles need to remain at a position during the hold period until the reach begins. During this early training phase, the learning rate can be quite high ( $1e-3$ ). Later, the CPN begins to learn the mapping between object shape information and the stimulation patterns needed to approximate the target grasp for that object. This later phase of training requires a learning rate 2-3 orders of magnitude lower than in the first phase ( $1e-6$  to  $5e-5$ ). See Section 4 for more details.

*3.3.4. Interleaved CPN/EN training, and adapting to non-stationarity* Having defined the training procedures for the EN and CPN, we can define a training protocol combining those two. We train the two in alternation, creating a new EN each time we enter an EN training phase. We explored the possibility of reusing an existing EN but found that retraining an EN was no more fast than training a new one. Training a new EN also allows us to adapt to the brain’s non-stationarity, which requires us to determine when the current EN is no longer suitable for training the current CPN. Our algorithm retires the current EN and trains a new one when one of two conditions is satisfied: (1) the EN’s prediction error is sufficiently above some fraction of the CPN’s task loss; or (2) if CPN loss does not improve (or gets worse) over a sufficient number of recent training steps (this is a common stopping criterion in machine learning). Additional details can be found in the Supplementary Materials section 7.3.

### 3.4. Experiments

We performed eight experiments to investigate the co-processor’s ability to learn under a variety of conditions. We studied three types of lesions to the cortical network model (simulated stroke) and for each lesion type, we turned on or off (a) brain/co-processor co-adaptation (brain recovery during co-processor use), (b) brain recovery *before* co-processor use, and (c) non-stationarity due to sensor drift during co-processor use. The

eight experiments are summarized in the following table (a blank entry under a condition (e.g., Co-adaptation?) means “No” while an X means “Yes”):

	<b>Lesion</b>	<b>Co-adaptation?</b>	<b>Prior recovery?</b>	<b>Sensor drift?</b>
1	50% AIP loss			
2	50% AIP loss	X		
3	50% M1 loss			
4	50% M1 loss	X		
5	100% connection loss F5<->M1			
6	100% connection loss F5<->M1	X		
7	100% connection loss F5<->M1	X	X	
8	100% connection loss F5<->M1	X		X

Each of the above experiments used the same set of input and output data as was used by Michaels et al. [30] to train the cortical model that we use. The dataset contains a total of 502 trials, sampled uniformly across 42 object classes. In each experiment, we held out a random sample of 20% of the dataset for validation.

### 3.5. Stopping criteria

In these experiments, we train the co-processor until one of the following two stopping criteria is satisfied (in Supplementary Materials section 7.7, we probe how these criteria affect the results). The two criteria are:

- The percent change in average task loss between two consecutive ranges of 500 epochs is below a threshold, indicating minimal benefits of further training. The choice of threshold varies by experiment, due to the significant differences in setup. See Supplementary Material section 7.7 for further details.
- The training run has exceeded some number of epochs. This also varied by experiment.

## 4. Results

For each lesioning experiment, we track two metrics to characterize the learning progress. First, we track the task loss, which is an MSE loss that measures the co-processor’s ability to restore movement towards the target trajectory. We compute the loss based on the error between the muscle velocity trajectory output by the lesioned cortical network model and the ground truth muscle velocity data from the Michaels et al. experiment [30]. In our results, we characterize this loss in terms of percent loss recovery, i.e., difference

between lesioned and healthy performance. Specifically the percent loss recovery metric is defined as:

$$\text{percent loss recovery} = \left(1 - \frac{L - L_{\text{healthy}}}{L_{\text{lesioned}} - L_{\text{healthy}}}\right) \times 100 \quad (6)$$

where  $L$  is the current task loss, and  $L_{\text{healthy}}$  and  $L_{\text{lesioned}}$  are the task losses before the lesion was applied and after the lesion was applied (but before any recovery) respectively. Thus 0% represents percent loss equal to the lesioned brain (prior to any recovery) while 100% represents percent loss equal to the healthy brain. Note that it is possible for this metric to become negative if current task loss  $L$  exceeds  $L_{\text{lesioned}}$  (e.g., if the stimulation is not beneficial and makes task performance worse than the performance with the lesioned brain).

Second, we measure the degree to which the lesioned cortical model, when coupled with the co-processor, successfully differentiates the grasps for different object classes. We compare the ratio of total variation to within-class variation of muscle velocities, for grasps executed by the lesioned and the healthy cortical network. We define the grasp separability metric  $S$  as:

$$S = \frac{\sigma_a}{\sigma_w} - \frac{\sigma_{a,h}}{\sigma_{w,h}} \quad (7)$$

where  $\sigma$  measures the mean standard deviation, across time, and across all data points in a given sample,  $\sigma_a$  is the standard deviation of a dataset, and  $\sigma_w$  is the average of the within-class standard deviations ( $h$  indicates healthy). An  $S$  value of 0.0 indicates that the grasps for the different object classes vary to the same degree as the healthy network. A negative value indicates the grasping motions are more similar between the object classes; likewise a positive value indicates the grasps are more dissimilar.

The grasp separability metric  $S$  allows us to differentiate between overall task performance improvement and the ability of the co-processor to condition the grasp on the input object based on visual information. To successfully grasp in the real world, the hand must be preformed appropriately for the shape of the object being grasped, and must close around it appropriately. Note that it is possible for the structure of the delayed reach-to-grasp task to be potentially learned by the co-processor, (e.g., to hold muscle velocities to 0.0 for the initial part of each trial) without learning to also differentiate the various object shapes.  $S$  provides a useful metric in this regard for tracking changes in grasp separability as opposed to only overall changes in task loss.

#### 4.1. Experiment 1: AIP 50% lesion

Our first experiment tested the ability of the co-processor to compensate for the loss of a significant fraction (50%) of the model neurons in the AIP module of the cortical model; this module is responsible for encoding object shapes from visual inputs. Loss of AIP model neurons results in the cortical model, without further adaptation, being unable to condition its grasp on the object shape, after largely succeeding in reaching

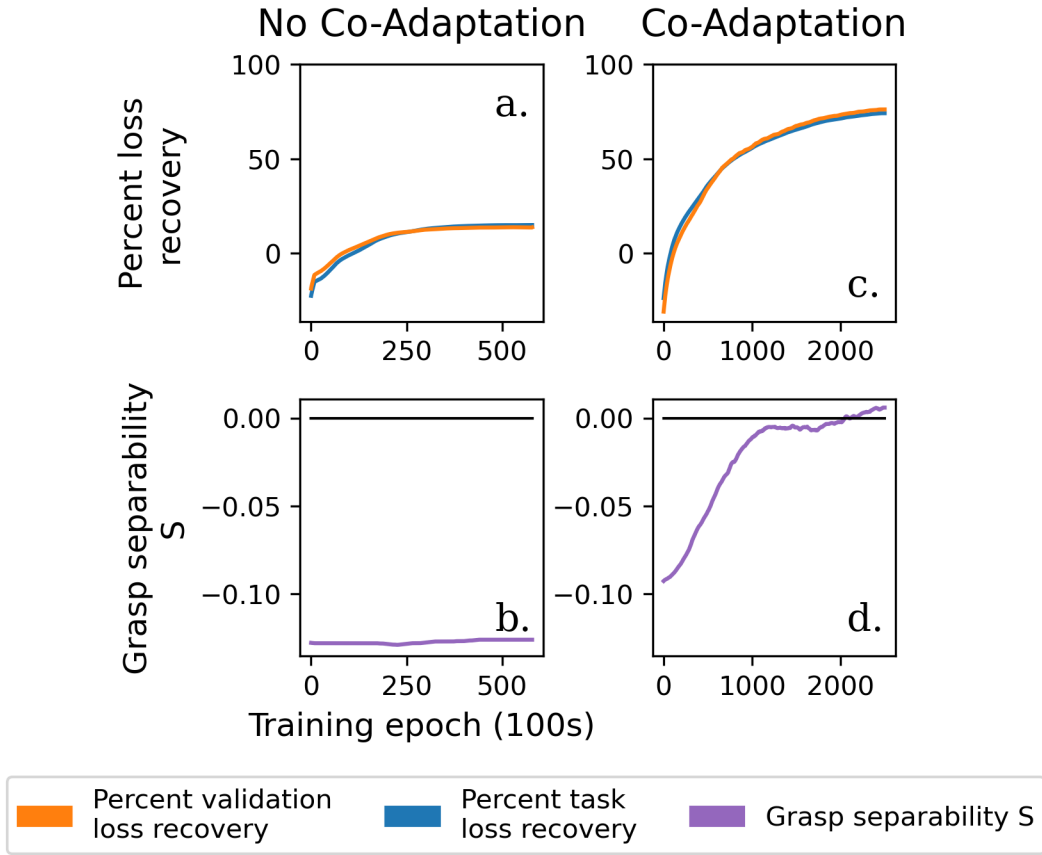


Figure 8: Co-Processor Performance Results: AIP 50% Lesion. a. Percent loss recovery for the non-coadaptive experiment for the task and validation datasets. 0% represents task loss equal to the loss for the lesioned cortical model, prior to any recovery. 100% represents loss equal to that for the healthy cortical model. Negative initial values are due to the newly-initialized CPN causing worse performance than the lesioned model prior to recovery. b. Grasp separability metric ( $S$ ) for the non-coadaptive experiment. Negative  $S$  values indicate grasps are more similar between object types while positive values indicate they are more distinct. c., d. show the performance of the neural co-processor for the co-adaptive experiment.

toward the object.|| Likewise, the co-processor cannot observe sufficient object shape encoding information due to the AIP lesion. As a result, as shown in Fig. 8a, significant recovery is not possible. Fig. 8b shows that the co-processor never learns to separate object classes ( $S$  value never approaches or exceeds 0.0).

In the co-adaptive case, the brain and co-processor together find a solution that reaches 76% recovery towards healthy performance. This demonstrates that the co-processor can adapt to the non-stationarity of the mapping between the muscle outputs and the CPN-delivered stimulation. As the brain adapts, it learns to encode the input

|| In Supplementary Materials section 7.9, lesioned loss is lower in this experiment than in others: the subject continues to reach successfully, but does not form the hand properly.

visual information, which in turn allows the co-processor to observe that information through its “recordings.” The co-processor can then leverage that information to condition stimulation, improving task performance (Fig. 8c). Note, though, that this simulation is not designed to indicate if the co-processor speeds up recovery, or provides better results than natural recovery, since we aren’t modeling the timeline of natural recovery. With this lesion design, simulated recovery would in-fact allow near-complete recovery of task performance. As a result, this experiment is designed only to demonstrate co-adaptation.

In Fig. 8d, which plots the grasp separability metric  $S$ , we see that initially the co-processor and the simulated brain do not strongly separate the object classes, resulting in negative  $S$  values, but as the co-processor training proceeds, the metric exceeds 0.0, indicating separability. This can be attributed to the co-processor and the simulated brain learning how to map the input visual information about object shape to the appropriate grasp for the object.

In Figs. 8a and c, the initial percent loss recovery values are negative: this is because the newly-initialized CPN in the co-processor delivers stimulation that initially causes task performance to be worse than the performance of the lesioned simulated brain; this is corrected with further training of the CPN.

#### 4.2. Experiment 2: M1 50% lesion

In this experiment, we lesioned 50% of the M1 module of the cortical model. As shown Fig. 9a, in the non-coadaptive case, training quickly plateaus at 75%, and does not improve thereafter. This suggests the lesion inactivated some of the degrees of freedom needed to control the output layer, resulting in a reduced ability to recreate the different target grasps for different objects (Fig. 9b).

In the co-adaptive case (Fig. 9c), performance likewise hits an inflexion point at 75%, but continues to improve slowly. The ability to improve further is tied to the “natural” recovery occurring in the co-adapting cortical model, which restores some of the degrees of freedom needed for improving grasping performance (Fig. 9d). The co-processor in this case adapts successfully to this non-stationarity being caused by the recovery process.

#### 4.3. Experiment 3: F5 and M1 connection lesion

In this experiment, we disconnected F5 from M1 completely to test whether the co-processor can act as a bridge between the two areas to appropriately convey information required for the grasping task from one area to the other. As in the other experiments, the co-processor’s task performance in this experiment improved quickly (Fig. 10a and c), but it took much longer to refine the stimulation patterns to enable object differentiation (Fig. 10b and d).

Since feedback from the output cannot “backpropagate” to the F5 and AIP modules, co-adaptation and learning in this experiment only affects the M1 module. As a result, the co-processor’s performance in this experiment demonstrates that its learning algorithm



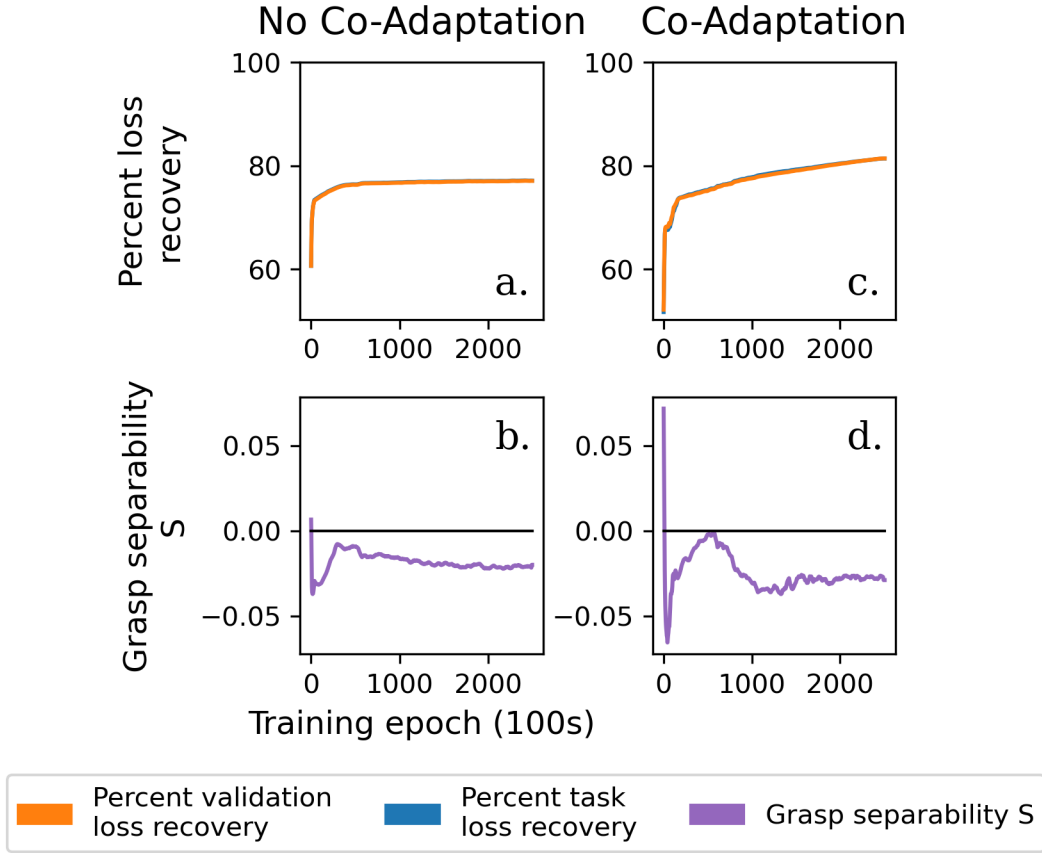


Figure 9: Co-Processor Performance Results: M1 50% Lesion. a. Percent loss recovery for the non-coadaptive experiment for the task and validation datasets. See caption for Fig. 8 for interpretation of positive and negative values. b. Grasp separability metric ( $S$ ) for the non-coadaptive experiment. See caption for Fig. 8 for interpretation of positive and negative values. c., d. show the performance of the neural co-processor for the co-adaptive experiment.

is capable of adapting to non-stationarity in the cortical model’s mapping between stimulation parameters and the behavioral output (muscle velocities for grasping). These results contrast with the results of Experiment 1, where the non-stationarity affected the mapping between the visual inputs and the AIP outputs.

As seen in Fig. 10b and d, grasp separation for objects is initially low and unstable, as the co-processor begins to learn the task, but later stabilizes as the co-processor begins to leverage observed brain activity to differentiate object shapes, gradually meeting or exceeding the pre-lesion grasping performance.

To illustrate the effect of the EN training dataset composition as described in section 3.3, we performed additional experiments on the F5-M1 connection lesion where we varied the dataset composition. As outlined in section 3.3), the training data set for the EN is composed of stimulation examples drawn from the current CPN, examples drawn from other CPNs with parameters in the neighborhood of the current CPN in parameter

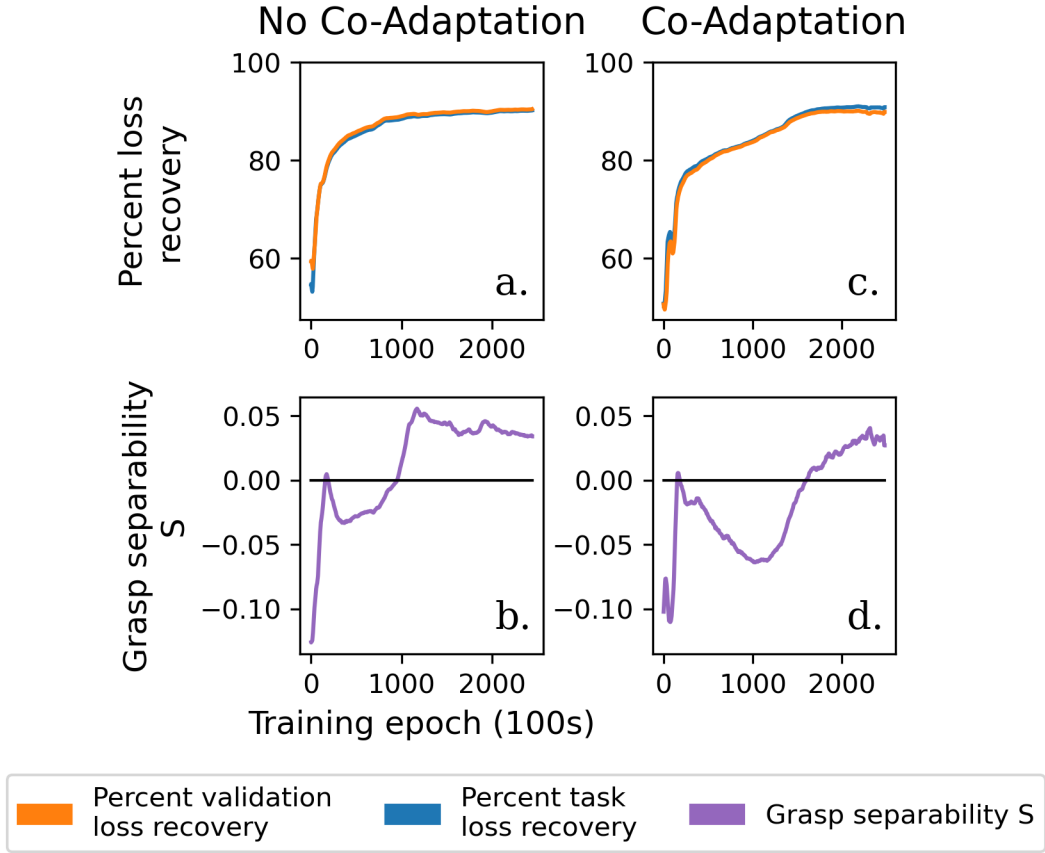


Figure 10: Co-Processor Performance Results: F5-M1 Connection Lesion. a. Percent loss recovery for the non-coadaptive experiment for the task and validation datasets. See caption for Fig. 8 for interpretation of positive and negative values. b. Grasp separability metric ( $S$ ) for the non-coadaptive experiment. See caption for Fig. 8 or interpretation of positive and negative values. c., d. show the performance of the neural co-processor for the co-adaptive experiment.

space (referred to as “exploratory examples”), and randomized stimulation. In Fig. 11, we see the effect of removing the latter two types of examples. Exploratory examples proved necessary to stabilize training, and to achieve higher levels of recovery. Removing the examples of randomized stimulation resulted in even more unstable training, where no improvement in task performance occurs.

#### 4.4. Experiment 4: Connection lesion with recovery

It is often the case that after a stroke, the brain recovers some of the function lost immediately after the stroke. We simulated this natural recovery in our cortical network model by lesioning the F5-M1 connections and then training the lesioned network on the grasping task. Complete recovery is impossible because the M1 module’s connections to F5 (both forward and backward) are disconnected. The cortical network model in

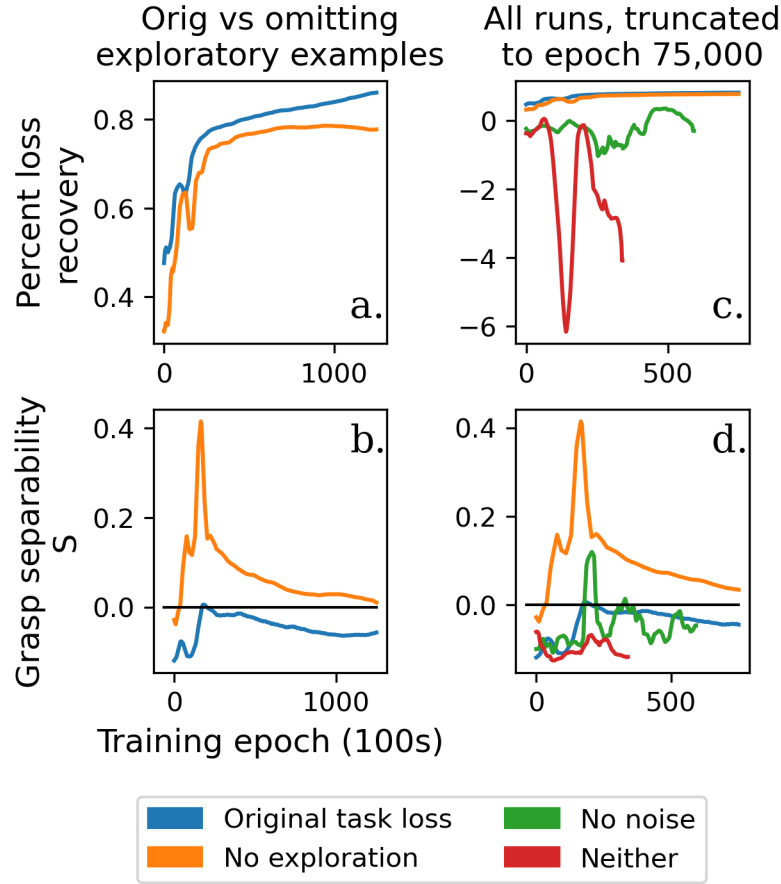


Figure 11: Co-Processor Performance Results: F5-M1 Connection Lesion: Use of exploratory and randomized examples in the training data set lead to stabilized and faster training. a., b. Without exploratory examples in the neighborhood of the CPN, we have unstable and slower training. In this case, the data set is composed of 10% examples drawn from the CPN, and 90% randomized examples (“No exploration”). c., d. Using only examples from the CPN (“Neither”; no exploratory or randomized examples) or 10% CPN and 90% exploratory examples (“No noise”; no randomized examples) also leads to unstable training. In c. and d., we truncate the experiments and use different axes to allow for clearer plots, but show the data from a. and b. for comparison.

this case learns an object-agnostic stereotypical grasp. We tested whether a co-processor can subsequently improve grasping performance beyond natural recovery by learning to convey to M1 via stimulation the object-related information from AIP and F5 necessary to tailor the grasp to the current input object’s shape.

We found that the co-processor can successfully improve task performance beyond the natural recovery after the simulated “stroke” (Fig. 12a). The dashed line indicates task loss after initial recovery. As in some experiments above, task performance is initially worse than after recovery, due to stimulation by an initially untrained co-processor. However the co-processor gradually learns to drive the task loss lower, as it

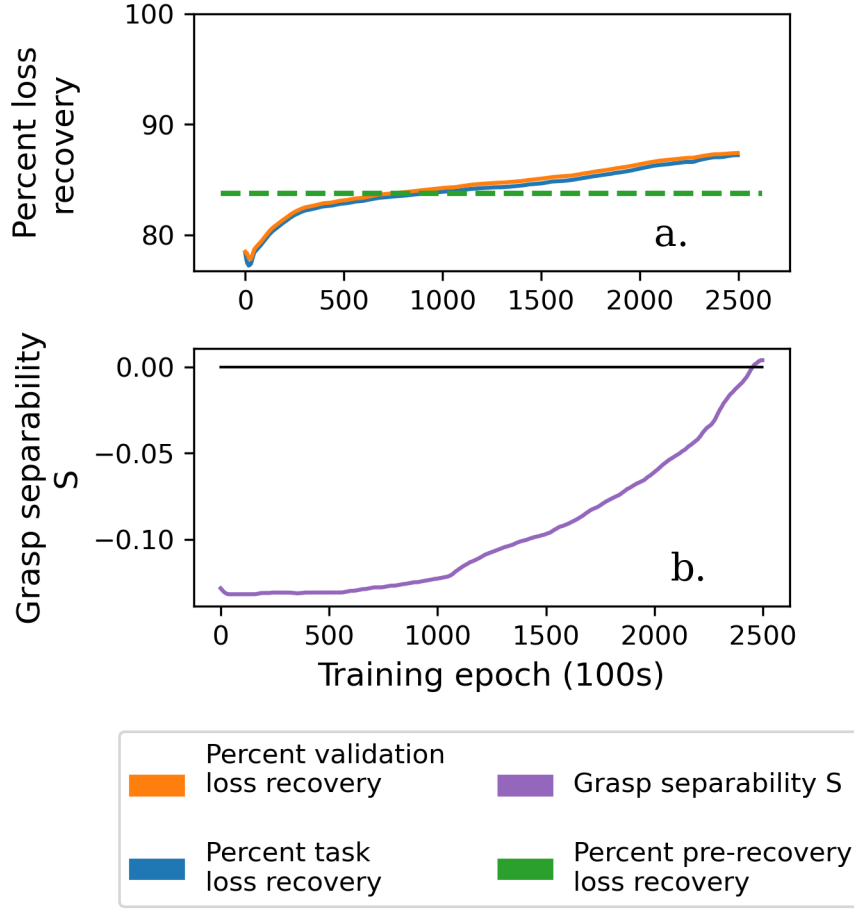


Figure 12: Co-Processor Performance Results: Connection Lesion and Natural Recovery before Co-Processor Use. a. Percent loss recovery for the task and validation datasets. The horizontal dashed line is the task performance after both lesioning and natural recovery but before co-processor use. Initially the co-processor’s stimulation causes task performance to be worse than the performance after natural recovery, but eventually the co-processor’s performance exceeds this level. b. Grasp separability metric ( $S$ ). Negative  $S$  values indicate grasps are more similar between object types while positive values indicate they are more distinct.

learns to forward-propagate information from the “earlier” parts (AIP and F5) of the simulated brain. Also, note that the grasp separation metric  $S$  returns to a healthy value towards the end of co-processor training (Fig. 12b).

#### 4.5. Experiment 5: Connection lesion with sensor drift

Sensor-related non-stationarities are often seen in real-world neural recording systems due to a variety of factors, from impedance changes due to sensor movement to scar tissue formation. In our final experiment, we again lesioned the F5-M1 connections and

allowed co-adaptation by the simulated cortical model but additionally, we allowed the sensor readings to drift over time. This drift was modeled in the recording function, where the readings had a non-stationary zero point across epochs. We added a bias term which we updated between epochs according to a random process (see Supplementary Materials section 7.4 for details).

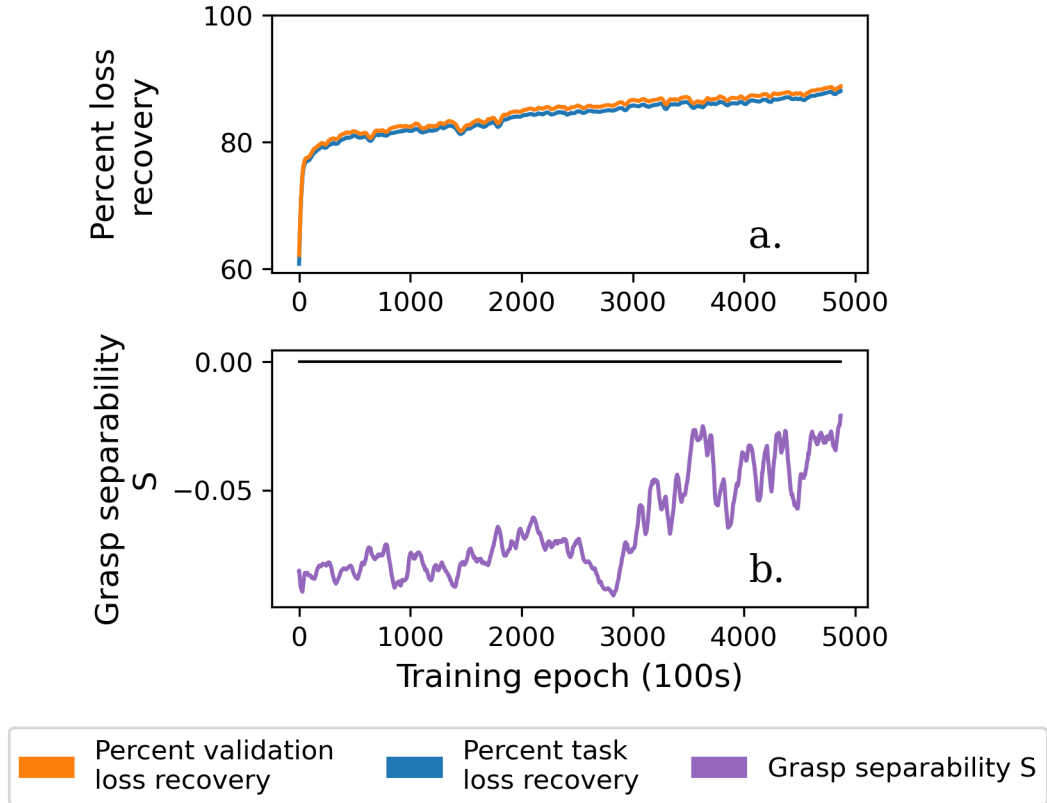


Figure 13: Co-Processor Performance Results: Connection Lesion with Sensor Drift. a. Percent loss recovery for the task and validation datasets. 0% represents task loss equal to the loss for the lesioned cortical model, prior to any recovery. 100% represents loss equal to that for the healthy cortical model. b. Grasp separability metric ( $S$ ) which reflects the co-processor’s ability to tailor grasps to specific objects. A negative value indicates the grasps are less differentiated between object shapes. Due to sensor drift, the co-processor is much slower to differentiate objects and the trend exhibits higher noise compared to other experiments.

As seen in Fig. 13, the co-processor was able to quickly recover the reach-to-grasp part of the task, and then gradually learned to condition the grasp on the object information.<sup>¶</sup> Because the recording model is non-stationary in this experiment, the object class separation exhibits far greater epoch-to-epoch variability in the later epochs.

<sup>¶</sup> Note that we relaxed our 250k epoch stopping criterion for these results because sensor drift causes a longer convergence time.

The co-processor presumably becomes more reliant on upstream visual information over time, as it learns to leverage this information in order to differentiate object shapes.

As expected, training efficiency was decreased relative to the experiment without sensor drift: with the sensor drift, 282K training epochs were needed to reach 85% recovery (Fig. 13a) while without sensor drift, only 93K were required (Fig. 10a).

## 5. Discussion and Future Work

We present here a first-of-its-kind demonstration of a novel design for neural co-processors, showing in simulation crucial training and design methodologies that lay the groundwork for co-processors to be demonstrated *in vivo* in the future. Our results show that a deep learning-based co-processor network (CPN) can learn neural stimulation policies that improve performance of an external task after simulated lesions in different parts of a cortical model. The training of the CPN relies on the use of a second neural network, called an emulator network (EN), which learns to approximate the function mapping stimulation and neural activity to task performance. Our experiments revealed the effects of different parameter choices and training paradigms for CPNs and ENs, providing new insights for future *in vivo* studies of neural co-processors.

Our co-processor design adapted well to a variety of simulated lesion types, reducing task loss 75 – 90% across our various experiments. The co-processor successfully adapted to the long-running dynamics of the simulated cortical model, as well as the long-range effects of stimulation. In some experiments, we required the co-processor to additionally adapt to non-stationarity in the neural circuit, which was actively changing at the same time the co-processor was learning. In one experiment, it also adapted to a simulated brain which had already undergone some amount of natural recovery after a lesion. In this case, the co-processor successfully identified the information upstream from the lesion which was necessary to stimulate the motor cortex (M1) module downstream. In the final experiment, the co-processor also successfully adapted to sensor drift simulated by a non-stationary recording model.

An important question that needs to be addressed is what can and cannot be inferred from simulation studies such as ours. Today, predicting neural responses to stimulation over long time scales and complex stimulation patterns remains a difficult problem, implying targeted control of neural activity is also difficult. Our simulation results do not constitute evidence that our method will, for example, immediately translate to restoration of fine-grained control for grasping in a stroke patient. One clear challenge is the sheer dimensionality of the problem. There exists a mismatch between the dimensionality of the brain and current sensor and stimulator technologies. We are also severely limited in the amount of training data which can reasonably be collected to train a closed-loop neural controller. We argue that while this fact clearly creates a challenge for learning-based closed-loop stimulation, the insights we have gained through our simulation studies are likely to be useful for *in vivo* testing of neural co-processors.

As mentioned in the Background section 2, it is important to test the feasibility

of applying a complex AI method such as a neural co-processor prior to testing it *in vivo*. Our simulations allowed us to design and test training methods around which future *in vivo* experiments can be developed. Additionally, iterating over different design choices in simulation minimizes the use of animal experimentation, supporting a commonly-accepted maxim regarding animal welfare in experimentation [31].

Our simulation studies required the co-processor to contend with issues of long-running dynamics and non-stationarity, which are likely to be key issues facing real-world *in vivo* deployments. We designed our training algorithm to contend with dimensionality by training the CPN with an EN that learns the effects of stimulation. The training algorithm adapts to non-stationarity by regularly updating the EN, allowing it to adapt to changes in the brain, in addition to “following” the CPN through stimulation parameter space. In the next section, we briefly explore the possibility of further addressing the dimensionality problem by using neural co-processors for optimizing low-dimensional neural correlates of task performance.

### 5.1. Co-processors for optimizing low-dimensional neural correlates of task performance

Though our simulation involves a neural co-processor directly optimizing stimulation for external task performance, the co-processor concept also generalizes to optimization for *neural correlates* (NCs) of task performance. We present this concept here to illustrate the generality of our approach, and to provide a possible path towards tackling the dimensionality issue. NCs are defined over measured brain activity and can be correlated with the desired patient outcome measures such as improved dexterity. If such a correlate additionally possesses a causal relationship to the patient outcome, i.e., if driving the NC through stimulation towards particular regimes also improves patient outcome, then it may serve as a co-processor’s optimization target. For example, Khanna et al. [23] suggest that “changes in task-related ensemble firing are linked to improvements in dexterity.” The authors then provide a measurement of ensemble co-firing which constitutes a candidate NC of dexterity and which may potentially be driven through stimulation.

A co-processor optimizing for an NCoD may provide a plausible path towards *in vivo* application. Driving a wide variety of grasping behaviors by altering the firing rates of a small number of individual neurons or multiunits may be infeasible in practice, and may not generalize well beyond the set of training examples. On the other hand, optimizing a neural correlate may generalize across a wide variety of behaviors. Additionally, such an optimization problem may be lower dimensional and require less training data in practice. We illustrate a design for such a co-processor in Fig. 14.

### 5.2. Future work

Identification of neural correlates such as NCoDs for different behaviors remains an open problem whose solution may enable efficient types of future co-processors. Similar to Khanna et al. [23], Heimbuch et al. recently presented work suggesting that there exist low-

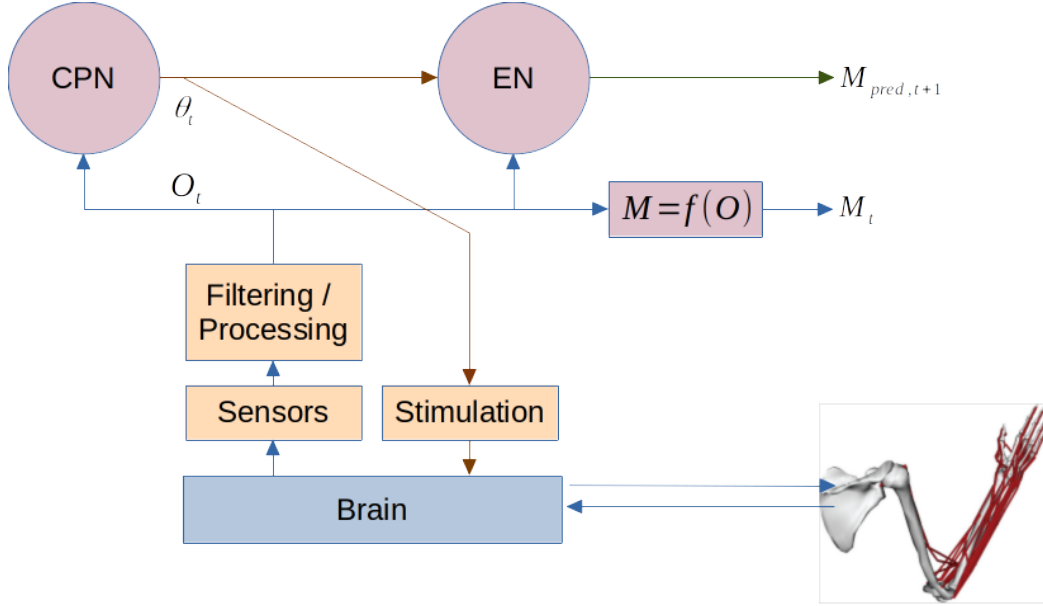


Figure 14: **A co-processor leveraging a neural correlate of dexterity rather than external (e.g., muscle) measurements.** Here, a measure  $M$ , serving as a neural correlate of dexterity, is calculated based on observed brain activity  $O$ . The emulator network (EN) learns to predict the future values of  $M$  as a function of  $O$  and stimulation parameters  $\theta$ . The co-processor network (CPN) maps the observed brain activity  $O$  onto stimulation parameters. The CPN is trained using the co-processor approach presented in this article with the objective of maximizing the dexterity measure  $M$  rather than minimizing a task loss defined in terms of grasping motions or muscle velocities.

dimensional neural correlates of dexterity which can be measured during and after stroke recovery [39]. They further hypothesize that neural stimulation could drive brain activity in a stroke patient towards maximization of those metrics, and that doing so would cause an improvement in dexterity. A co-processor could allow us to test these hypotheses by attempting to learn a CPN stimulation policy which optimizes the candidate NCoDs. Future work will involve collaborations with experimental neuroscientists to identify candidate NCs of desirable behavior, and to perform *in vivo* experiments involving co-processors that seek to optimize these NCs.

Additional future work will explore reinforcement learning (RL) approaches to training co-processors: the neural co-processor we explored in this article already includes a “policy network” (the CPN) and a “world model” (the EN). The proposed framework is therefore well-suited to model-based reinforcement learning algorithms such as model-based Actor-Critic learning. We will explore optimizing reward functions that involve not only symptom relief, but also minimizing energy use by attaching a cost to stimulation.

One additional challenge remaining with our current co-processor design is data efficiency. On the whole, the co-processor quickly improved task performance, but required orders of magnitude more training examples to achieve its highest levels of



performance. Even moderate amounts of recovery may be valuable to a user, but nevertheless we consider data efficiency to remain a problem. Due to limits on patient fatigue, time, implant battery life, and other concerns, it is not plausible to expect a learning algorithm to have access to unlimited amounts of training data. As a result, it is necessary to make efficient use of the data we can acquire. We believe there exist at least four mitigation strategies for this:

- Retraining an existing EN, rather than repeatedly creating a new one. As mentioned above, the former approach did not yield good results, but it remains to be seen if this is a fundamental problem with our training method or a peculiarity of our simulation which we have yet to identify. This remains a future area of inquiry.
- Making better use of what data we acquire. In this initial simulation, we do not retain data beyond the present training epoch because non-stationarity requires us to regularly discard data as it ages. We found that in the presence of a rapidly learning CPN, and especially in our co-adaptive experiments, data retention in fact caused training instability. However, in practice, training epochs operate on the order of seconds, suggesting that data could be retained and reused for multiple epochs. The “speed” of non-stationarity compared to the co-processor’s learning is an area worthy of future investigation.
- Matching the dimensionality of the stimulation parameters and the optimization target to the amount of available data. A stimulation paradigm with a small number of controllable parameters that nevertheless allows improvements in task performance will likely require less training data. Likewise, optimizing low-dimensional targets (e.g., NCoDs) may require less training data.
- Sharing data across subjects and transfer learning. Recent work has shown that it is possible to train a deep neural network using data from multiple subjects and transfer that knowledge to decode neural data from new subjects [40]. A similar technique could potentially be used to train ENs, reducing the amount of data needed from a new subject and improving data efficiency.

## 6. Conclusion

Using a simulated model of cortical circuits in the primate brain that are involved in grasping behaviors, we demonstrated a training method based on deep learning for a closed-loop neural stimulator called a “neural co-processor” [15, 16]. We created a learning paradigm which allowed the co-processor to adapt to the distributed neural activity in the simulated brain, as well as to the non-stationarity of the neural activity and the sensors, key properties which are likely necessary for future *in vivo* applications. We showed that the co-processor could be trained to restore grasping function after we applied varying types of simulated lesions. Specifically, a neural co-processor can be trained using deep learning through backpropagation with the help of two networks: a co-processor network (CPN) that learns to generate stimulation patterns to optimize

task performance, and an emulator network (EN) that learns to predict the effects of stimulation. Though the results we presented involved optimization of an external task, we believe that neural co-processors will successfully generalize to the optimization of neural correlates of health, successfully driving neural activity towards target regimes which are known to correlate with positive clinical outcomes. Given the generality of the framework, we expect neural co-processors to be applicable to a wide range of clinical applications that require adaptive closed-loop neural stimulation for treating sensorimotor disorders and neuropsychiatric conditions.

### Code and data availability

Code including analysis code used to generate figures can be found at <https://github.com/mmattb/coproc-poc>. Data is available upon reasonable request to the authors.

### Conflict of interest

The authors of this work are not aware of any conflicts of interest related to it.

### Acknowledgements

This work was supported by a Weill Neurohub Investigator grant, a CJ and Elizabeth Hwang endowed professorship (RPNR), National Science Foundation (NSF) grant no. EEC-1028725 and NSF EFRI grant no. 2223495. The authors would like to thank Karunesh Ganguly (UC San Francisco), Priya Khanna (UC Berkeley), Anca Dragan (UC Berkeley), Justin Ong, Ian Heimbuch, and Luciano De La Iglesia for discussions and insights related to this work.

### References

- [1] Rao R P N 2013 *Brain-Computer Interfacing: An Introduction* (Cambridge University Press) ISBN 9780521769419
- [2] Wolpaw J and Wolpaw E W 2012 *Brain-Computer Interfaces: Principles and Practice* (Oxford University Press)
- [3] Moritz C T, Ruther P, Goering S, Stett A, Ball T, Burgard W, Chudler E H and Rao R P N 2016 *IEEE transactions on bio-medical engineering.* **63**(7) 1354–1367 New perspectives on neuroengineering and neurotechnologies: Nsf-dfg workshop report
- [4] Lebedev M A and Nicolelis M A L 2017 *Physiological reviews* **97**(2) 767–837 Brain-machine interfaces: From basic science to neuroprostheses and neurorehabilitation
- [5] Walker E Y *et al.* 2019 *Nature Neuroscience* **22**(12) 2060–2065 Inception loops discover what excites neurons most using deep predictive models URL <https://doi.org/10.1038/s41593-019-0517-x>
- [6] Niparko J K 2009 *Lippincott Williams and Wilkins* (Oxford University Press)
- [7] Weiland J D and Humayun M S 2014 *IEEE transactions on bio-medical engineering* **61**(5) 1412–1424 Retinal prosthesis
- [8] Tomlinson T and Miller L E 2016 *Advances in experimental medicine and biology* **957** 367–388 Toward a proprioceptive neural interface that mimics natural cortical activity

- [9] Tabot G A, Dammann J F, Berg J A, Tenore F V, Boback J L, Vogelstein R J and Bensmaia S J 2013 *Proceedings of the National Academy of Sciences* **110** 18279–18284 Restoring the sense of touch with a prosthetic hand through a brain interface ISSN 0027-8424 (*Preprint* <https://www.pnas.org/content/110/45/18279.full.pdf>) URL <https://www.pnas.org/content/110/45/18279>
- [10] Tyler D J 2015 *Current opinion in neurology* **28**(6) 574–581 Neural interfaces for somatosensory feedback: bringing life to a prosthesis
- [11] Dadarlat M C, O’Doherty J E and Sabes P N 2015 *Nature neuroscience* **18**(1) 138–144 A learning-based approach to artificial sensory feedback leads to optimal integration
- [12] Flesher S N, Collinger J L, Foldes S T, Weiss J M, Downey J E, Tyler-Kabara E C, Bensmaia S J, Schwartz A B, Boninger M L and Gaunt R A 2016 *Science Translational Medicine* **8** 361ra141–361ra141 Intracortical microstimulation of human somatosensory cortex (*Preprint* <https://www.science.org/doi/pdf/10.1126/scitranslmed.aaf8083>) URL <https://www.science.org/doi/abs/10.1126/scitranslmed.aaf8083>
- [13] Cronin J A, Wu J, Collins K L, Sarma D, Rao R P N, Ojemann J G and Olson J D 2016 *IEEE transactions on haptics* **9**(4) 515–522 Task-specific somatosensory feedback via cortical stimulation in humans
- [14] O’Doherty J, Lebedev M, Ifft P, Zhuang K, Shokur S, Bleuler H and Nicolelis M 2011 *Nature* **479**(7372) 228–231 Active tactile exploration using a brain–machine–brain interface URL <https://doi.org/10.1038/nature10489>
- [15] Rao R P N 2019 *Current Opinion in Neurobiology* **55** 142–151 Towards neural co-processors for the brain: Combining decoding and encoding in brain-computer interfaces
- [16] Rao R P N 2020 Brain co-processors: Using AI to restore and augment brain function *Handbook of Neuroengineering* ed Thakor N (Springer)
- [17] Yang Y, Qiao S, Sani O, Sedillo J, Ferrentino B, Pesaran B and Shanechi M 2021 *Nature Biomedical Engineering* **5**(4) 324–345 Modelling and prediction of the dynamic responses of large-scale brain networks during direct electrical stimulation URL <https://doi.org/10.1038/s41551-020-00666-w>
- [18] Tafazoli S, MacDowell C, Che Z, Letai K, Steinhardt C and Buschman T 2020 *Journal of Neural Engineering* **17** 056007 Learning to control the brain through adaptive closed-loop patterned stimulation URL <https://doi.org/10.1088/1741-2552/abb860>
- [19] Benabid A 2003 *Current opinion in neurobiology* **13**(6) 696–706 Deep brain stimulation for parkinson’s disease
- [20] Holtzheimer P and Mayberg H 2011 *Annual review of neuroscience* **34** 289–307 Deep brain stimulation for psychiatric disorders
- [21] Kisely S, Hall K, Siskind D, Frater J, Olson S and Crompton D 2014 *Psychological medicine* **44**(16) 3533–3542 Deep brain stimulation for obsessive-compulsive disorder: a systematic review and meta-analysis
- [22] Frait A and Pal G 2015 *Frontiers in Neurology* **6** 170 Deep brain stimulation in tourette’s syndrome ISSN 1664-2295 URL <https://www.frontiersin.org/article/10.3389/fneur.2015.00170>
- [23] Khanna P, Totten D, Novik L, Roberts J, Morecraft R and Ganguly K 2021 *Cell* **184**(4) 912–930 Low-frequency stimulation enhances ensemble co-firing and dexterity after stroke URL <https://pubmed.ncbi.nlm.nih.gov/33571430/>
- [24] Bosking W, Beauchamp M and Yoshor D 2017 *Annual review of vision science* **3** 141–166 Electrical stimulation of visual cortex: Relevance for the development of visual cortical prosthetics
- [25] Castaño-Candamil S, Ferleger B I, Haddock A, Cooper S S, Herron J, Ko A, Chizeck H J and Tangermann M 2020 *Frontiers in Human Neuroscience* **14** 421 A pilot study on data-driven adaptive deep brain stimulation in chronically implanted essential tremor patients URL <https://www.frontiersin.org/article/10.3389/fnhum.2020.541625>
- [26] Little S e a 2016 *Journal of neurology, neurosurgery, and psychiatry* **87**(7) 717–21 Bilateral adaptive deep brain stimulation is effective in parkinson’s disease.

- [27] Berger T W, Song D, Chan R H M, Marmarelis V Z, LaCoss J, Wills J, Hampson R E, Deadwyler S A and Granacki J J 2012 *IEEE transactions on neural systems and rehabilitation engineering : a publication of the IEEE Engineering in Medicine and Biology Society* **20**(2) 198–211 A hippocampal cognitive prosthesis: multi-input, multi-output nonlinear modeling and vlsi implementation
- [28] Kahana M J e a 2021 *medRxiv* Biomarker-guided neuromodulation aids memory in traumatic brain injury (*Preprint* <https://www.medrxiv.org/content/early/2021/05/22/2021.05.18.21256980.full.pdf>) URL <https://www.medrxiv.org/content/early/2021/05/22/2021.05.18.21256980>
- [29] Bolus M, Willats A, Rozell C and Stanley G 2021 *Journal of neural engineering* **18**(3) State-space optimal feedback control of optogenetically driven neural activity
- [30] Michaels J, Schaffelhofer S, Agudelo-Toro A and Scherberger H 2020 *Proceedings of the National Academy of Sciences* **117** 32124–32135 A goal-driven modular neural network predicts parietofrontal neural dynamics during grasping ISSN 0027-8424 (*Preprint* <https://www.pnas.org/content/117/50/32124.full.pdf>) URL <https://www.pnas.org/content/117/50/32124>
- [31] Council N R 2011 *Guide for the Care and Use of Laboratory Animals: Eighth Edition* (Washington, DC: The National Academies Press) ISBN 978-0-309-15400-0 URL <https://nap.nationalacademies.org/catalog/12910/guide-for-the-care-and-use-of-laboratory-animals-eighth>
- [32] Dura-Bernal S, Li K, Neymotin S, Francis J, Principe J and Lytton W 2016 *Frontiers in Neuroscience* **10** 28 Restoring behavior via inverse neurocontroller in a lesioned cortical spiking model driving a virtual arm ISSN 1662-453X URL <https://www.frontiersin.org/article/10.3389/fnins.2016.00028>
- [33] Kim L Y, Harer J A, Rangamani A, Moran J, Parks P D, Widge A S, Eskandar E N, Dougherty D D and Chin S P 2016 *2016 38th Annual International Conference of the IEEE Engineering in Medicine and Biology Society (EMBC)* 808–811 Predicting local field potentials with recurrent neural networks
- [34] Güçlü U and van Gerven M 2017 *Frontiers in computational neuroscience* **11** Modeling the dynamics of human brain activity with recurrent neural networks.
- [35] Sussillo D, Churchland M, Kaufman M and Shenoy K 2015 *Nature Neuroscience* **18**(7) 1025–1033 A neural network that finds a naturalistic solution for the production of muscle activity
- [36] Simonyan K and Zisserman A 2015 Very deep convolutional networks for large-scale image recognition *International Conference on Learning Representations*
- [37] Puthenveetil S, Fluet G, Qiu Q and Adamovich S 2012 *Annual International Conference of the IEEE Engineering in Medicine and Biology Society. IEEE Engineering in Medicine and Biology Society. Annual International Conference* **2012** 4563–4566 Classification of hand preshaping in persons with stroke using linear discriminant analysis.
- [38] Loshchilov I and Hutter F 2017 *arXiv preprint arXiv:1711.05101* Decoupled weight decay regularization
- [39] Heimbuch I, Khanna P, Novik L, Morecraft R and Ganguly K 2022 Changes in somatosensory and premotor cortex neurophysiology during recovery of reach-to-grasp control following motor cortex stroke *Society for Neuroscience* URL [https://www.sfn.org/-/media/SfN/Documents/NEW-SfN/Meetings/Neuroscience-2022/Abstracts/Abstract-PDFs/SFN22\\_Abstracts-PDF-Nano.pdf](https://www.sfn.org/-/media/SfN/Documents/NEW-SfN/Meetings/Neuroscience-2022/Abstracts/Abstract-PDFs/SFN22_Abstracts-PDF-Nano.pdf)
- [40] Peterson S M, Steine-Hanson Z, Davis N, Rao R P N and Brunton B W 2021 *Journal of Neural Engineering* **18** 026014 Generalized neural decoders for transfer learning across participants and recording modalities URL <https://dx.doi.org/10.1088/1741-2552/abda0b>
- [41] Martens J and Sutskever I 2011 *Proceedings of the 28th International Conference on Machine Learning (ICML-11)* 1033–1040 Learning recurrent neural networks with hessian-free optimization
- [42] Kao J 2019 *Journal of Neurophysiology* **122** 2504–2521 Considerations in using recurrent neural

networks to probe neural dynamics URL <https://doi.org/10.1152/jn.00467.2018>

## 7. Supplementary Materials

### 7.1. Details of the simulated task

The reach-to-grasp task on which the mRNN cortical model was trained involves multiple phases, which can be identified by the mRNN’s inputs. Initially, the NHP subject sat in a dark room, with only a red cue visible. After a short period, an object was presented to the subject visually, after which the overhead light was turned off and once again only the red cue was visible. After another brief period, the red cue was turned off, which cued the subject to perform a grasp and hold of the object (still in the dark). This task is presented in more detail in the work of Sussillo [35] and Michaels et al. [30].

The inputs to the mRNN network encode the task phase information. It consists of a twenty dimensional vector of visual features, which are presented only to the input (AIP) end of the network, and a 1D hold signal, which is presented to all neurons across the network. The authors of Michaels et al. [30] derived the hold signal from the grasp data, and it represents a point in time shortly before grasping began. As explained above, the visual features are drawn from VGGNet [36], based on rendered images. The images consist of some combination of the red cue light and the object image. Note that the visual input vector and hold signal are not observed directly by the co-processor, but rather indirectly via brain recordings.

The phases of the task are depicted in Table 1, and the timeline of a single trial is depicted in Fig. 15.

Description	Cue	Object image	Hold signal
A rest period, during which a red cue light is presented	On	Off	On
The object presentation period, during which the image of the object and cue are visible	On	On	On
A rest period	On	Off	On
Cue is turned off	Off	Off	On
Subject performs grasp	On	Off	Off

Table 1: **Phases of the reach to grasp task.** During each phase, a visual stimulus as well as a binary hold signal are presented. The visual stimulus encodes an image, consisting of a red cue light and/or an image of an object.

### 7.2. Training the cortical model for grasping

For our simulation, we leverage a pre-trained mRNN cortical model, provided by the lead author of Michaels et al. [30] and used with their permission. The training method for that model is based on prior work by the same authors, and others [35].

Training involved the use of Hessian-free optimization [41], rather than the more common first-order stochastic gradient descent. Additionally, an L2 firing rate

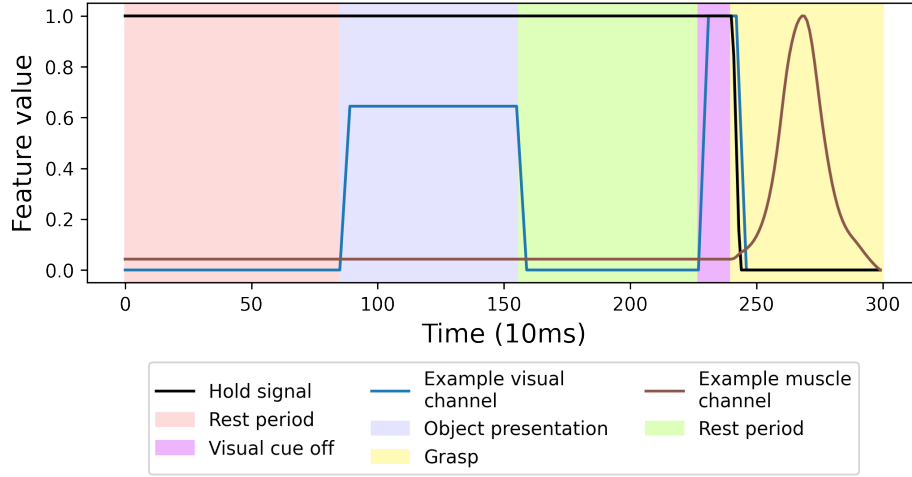


Figure 15: Timeline of a Single Trial

regularization, and an L2 input and output model weight regularization were used. These regularizations are believed to result in more biologically plausible RNNs [42].

The authors varied the model’s nonlinearities, regularization weights, and inter-module sparsities. Among those, we chose one model arbitrarily for our study. Specifically, the model we chose was structured, and trained using:

- The rectified hyperbolic tangent nonlinearity
- $1e-1$  Inter-module sparsity
- $1e-3$  L2 firing rate regularization
- $1e-5$  L2 weight regularization

### 7.3. EN/CPN Interleaving

We train a CPN until an EN is no longer useful. At that point we train a new EN. We deem an EN as no longer useful if one of the following predicates becomes true:

- The EN prediction loss is greater than  $\min(6e-4, L/10)$ , where  $L$  is the most recent task loss. EN prediction loss is an MSE loss between the EN’s prediction of muscle velocities, and the actual muscle velocities output by the grasping model network.
- Task loss increased across 15 of the previous 30 training epochs.
- 100 CPN training epochs have elapsed.

Likewise, the EN training period ends when its prediction loss  $L$  on the validation data set drops below a threshold of  $\max(3e-4, L/50)$ .

### 7.4. Sensor drift

To simulate sensor drift, we add a vector to a bias term introduced to the recording function. We draw the elements of the vector from a zero-mean Gaussian distribution,

with variance based on the mean value of the recording function from prior connection-lesion experiments. That allows us to put it into a reasonable range, where it is effective but not extreme. We attempted the experiment with several values of the variance, and found the results to be principally the same: the co-processor eventually learned, but at a rate slower than otherwise. We present results for a variance of  $1.5e-3$ , which is 2% of the mean recording value.

### 7.5. Passthrough reference model

To understand the effect of the recording and stimulation functions on the co-processor’s performance, we repeated our experiment with the F5-M1 connection lesion and coadaptation using passthrough recording and stimulation functions. “Passthrough” here means that the recording and stimulation functions have dimensionality equal to the number of neurons we are recording from or stimulating, respectively, and that there is no temporal or spatial smoothing used. That allows the co-processor to directly observe the hidden state of the AIP and F5 neurons in the simulated grasping circuit, and to directly influence the hidden state of the neurons in M1 it stimulates.

For this passthrough version of the experiment, we additionally increased the number of artificial neurons making up the CPN and EN, to account for the additional dimensionality of the inputs and outputs. Specifically, we increased the CPN from 61 to 200 neurons, and the EN from 87 to 351. We measured whether the increase in neurons alone caused the different results we see here, and found it did not; we omit those results for brevity.

In Fig. 16 we see that the co-processor performed significantly better with the passthrough functions. It learned faster, and to a higher recovery level: 97% compared with 90%. Note: we truncate the results to the point we stopped the passthrough experiment. The reader can find the final results in Supplementary Materials 7.9.

### 7.6. Effect of observability on the recording function and training results

To study the effect of brain observability on the co-processor’s training behavior we repeated the co-adaptive connection lesion experiment (4.3) with varying recording functions. Here we varied the number of simulated electrodes in each mRNN module, and additionally performed an experiment with a passthrough recording function, as described in the prior section. Specifically, our original experiment used 20 electrodes per module. Our additional experiments include 1, 10, and 60 electrodes per module, and the passthrough recording function. This allows us to explore any gradient in the co-processor training results with respect to observability of the brain. Additionally, we reduced the variance of the Gaussian governing the sensor model, such that an experiment with e.g. 1 electrode per module measures effectively only 1-2 neurons per module. We held the number of neurons making up the CPN and EN fixed across these variations to ensure we are examining the effects of the recording function alone. We



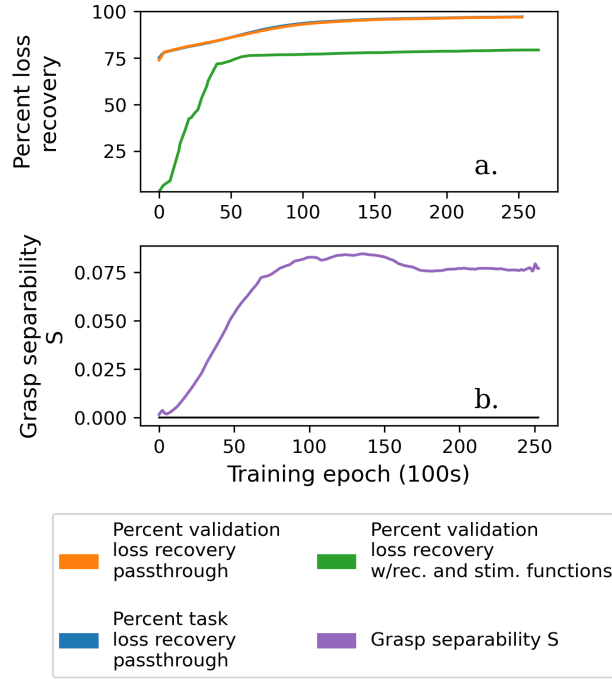


Figure 16: **Training Results: passthrough recording and stimulation functions.** The significantly faster training and higher recovery suggest the recording and stimulation functions make the task more difficult for the co-processor.

continued to stop learning at the point of 90% recovery or a slow rate of recovery. In Fig. 17 we present the results.

We did not experiment with the placement of the electrodes, i.e. varying their location among the neurons. It wasn't necessary to do so for the purpose of this experiment. However, it's conceivable that results could improve considerably if we happened to observe a small handful of key neurons.

Overall, learning is effectively the same regardless of the recording function, up to the point that only a small number of neurons can be observed. In all cases except the case of a single electrode, the co-processor learned to improve task performance to the 90% recovery point. Some variation in learning efficiency occurred, and perhaps notably the experiments with 1 and 10 electrodes observed the lowest two rates of recovery. The passthrough function and 60 electrode model observed the fastest recovery rates. Without additional computational power it remains difficult to hypothesis test the effect of electrode count against learning efficiency, but the results suggest that small variations in electrode count away from the count of 20 used in our main experiments would not cause drastically different results.

Class separation behavior remained largely the same across these variations. The one exception is the experiment involving only 1 electrode per module. In that case, the co-processor learned to treat the object classes similarly. That suggests that the classes

could not be differentiated by the small amount of information attainable from a single electrode. In this case, the co-processor reduced towards a simpler closed-loop stimulator which modulates its behavior entirely on the user’s volition to initiate movement, due to the hold signal being observable from every neuron.

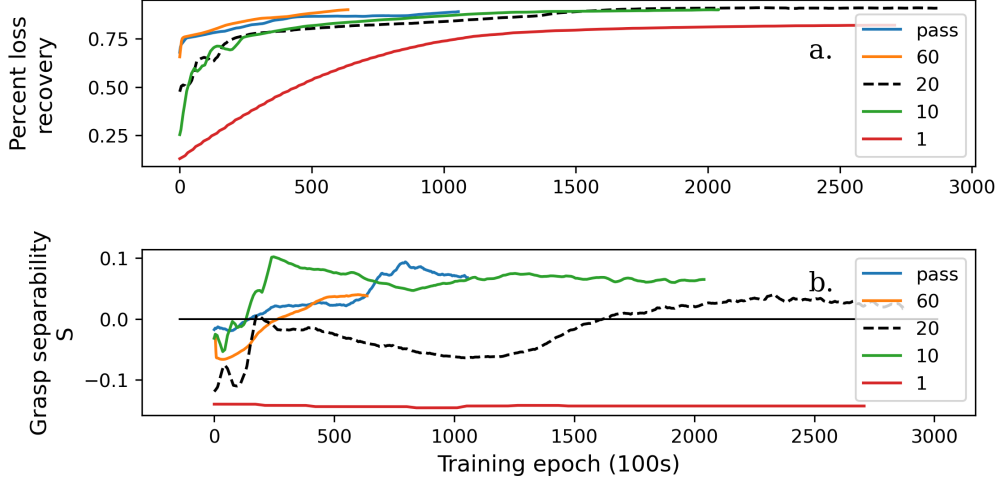


Figure 17: **Training Results: varying observability of the brain.** (a) Increasing observability of the brain leads to faster learning. Here we show results with a single simulated recording electrode in each module “1”, compared with “20” electrodes for the results reported in the main portion of this paper, and compared with other electrode counts. “pass” refers to a passthrough recording function where every simulated neuron was directly measured. Note that learning is generally the same as observability increases, though perhaps somewhat faster. We did not hypothesis test that effect. In all cases except “1”, learning reached a 90% recovery threshold where we stop training. (b) As in our connection-based lesion experiment above (4.3), class separation initially varied, then trended towards the separation exhibited by the healthy mRNN network. However, in the single electrode experiment “1”, class separation steadily decreased, suggesting that the information necessary to perform class separation cannot be determined from the information available to the single electrode.

### 7.7. Stopping criteria

Both stopping criteria affected the results presented above. We cannot economically perform statistical analysis to show e.g. the percentage of runs of each experiment type which are stopped by one criteria versus the other. However, in Table 2 we present the stopping criterion which caused the end of each experiment whose results we presented herein.

We used an alternate stopping condition for the sensor drift experiment, since recovery improved more slowly in that experiment due to the sensor drift. We allowed the experiment to run until roughly 500k epochs - essentially double the 250k epoch

criterion.

We also used an alternate stopping condition for the passthrough functions experiment. This was due to the computational expense: running the models at full resolution required far greater run time. As a result, we stopped this experiment once 97% recovery on the validation data was achieved.

Experiment	Loss change % (default: 0.1%)	Run length (default: 250k epochs)	Notes
AIP No-coadapt	X		
AIP Coadapt		X	
M1 No-coadapt		X	Pct change criteria relaxed to show longer-run S trend
M1 Coadapt		X	
Con No-coadapt	X		Loss chg threshold: 0.05%
Con Coadapt		X	Loss chg threshold: 0.05%
Recovery		X	
Sensor drift	X		Allowed to run to $\sim 500$ k epochs, due to slower convergence.
Passthrough			Stopped at 97% recovery, due to computational expense.

Table 2: **Stopping criterion which bound each experiment.** “Coadapt” refers to co-adaptation. “Con” refers to F5-M1 connection lesions. “Recovery” refers to the experiment involving recovery prior to co-processor training.

### 7.8. Prediction Accuracy of Stimulation Model (EN)

As mentioned in Section 3.3.2 above, we train our stimulation model, i.e. EN, to a high level of predictive power before using it to train the CPN. We expire it and create a new one when training performance begins to suffer, or prediction error significantly disimproves. To depict the EN’s predictions visually, Fig. 18 shows example muscle velocities for a highly trained CPN and EN, for one example output channel.

In Fig. 19 we see the variability of prediction losses across muscle channels. Prediction loss typically varies  $\pm 34.0\%$  for a given channel across all trials. Variability is roughly consistent across channels, suggesting that the statistic is not driven by extrema. However, there exist a handful of channels with high coefficients of variation (CVs). Those appear to be the channels with the lowest overall prediction losses, suggesting their CVs are driven by the low mean, rather than an unusually high variability.

### 7.9. Table of losses and recovery

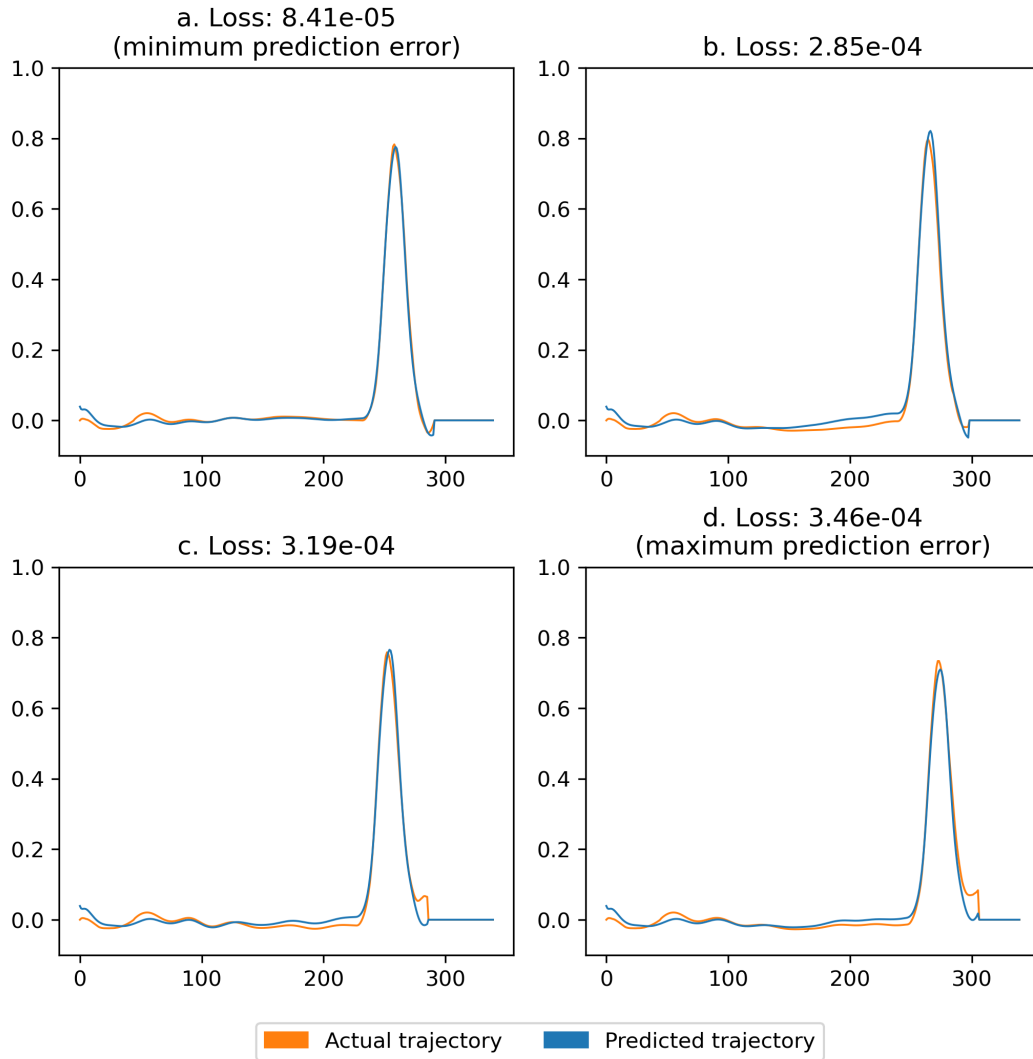
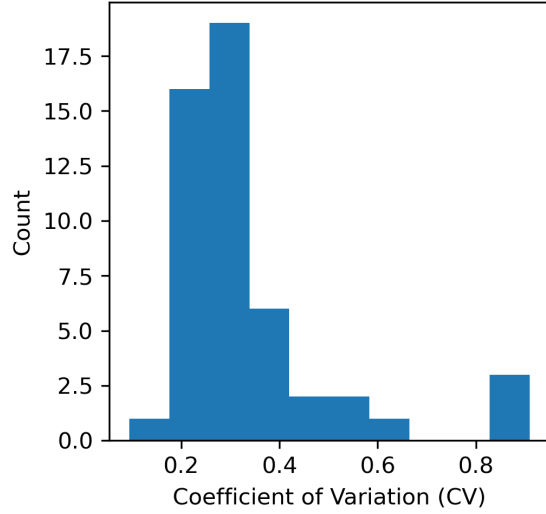
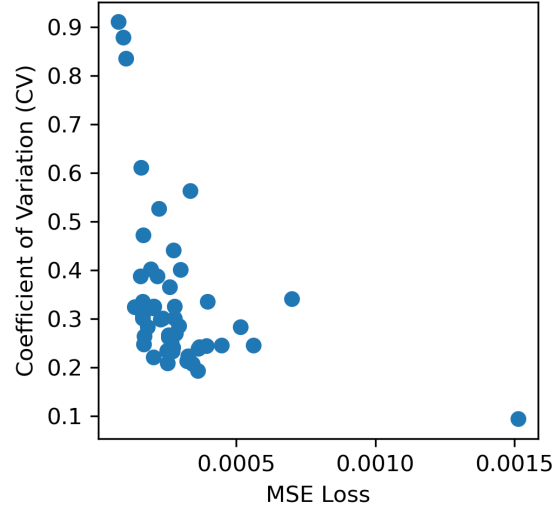


Figure 18: **Prediction errors for four trials, on TMAJ muscle (retracts the shoulder).** The EN's predicted trajectory for the TMAJ muscle (blue), closely tracks the actual trajectory (orange). Sourced from the co-adaptive connection lesion experiment. (a) depicts the trial with minimum prediction MSE. (d) maximum prediction MSE. (b, c) two other arbitrary-chosen trials. Standard deviation across all trials:  $1.91 \times 10^{-5}$ .



(a) **Histogram of coefficients of variability (CVs) across prediction MSE losses for each muscle channel.** Mean: 0.340; i.e. per-channel loss typically varies  $\pm 34.0\%$ .



(b) **Prediction MSE loss vs CV for each channel.** High CV extrema are from channels with the lowest losses. i.e. the highest CV values in (a) are due to extreme low losses, suggesting their CVs are driven by the low mean, rather than an unusually high variability.

Figure 19: **Prediction loss variability across muscle channels**

Experiment	Lesioned loss	Min task loss	Min task val loss	Pct recov	Pct recov val
AIP No-coadapt	0.004507	0.003916	0.003960	15.01%	13.89%
AIP Coadapt	0.004507	0.001575	0.001502	74.23%	76.26%
M1 No-coadapt	0.021136	0.005765	0.005604	74.73%	75.51%
M1 Coadapt	0.021136	0.004383	0.004385	81.39%	81.41%
Con No-coadapt	0.020719	0.002540	0.002490	90.21%	90.45%
Con Coadapt	0.020719	0.002350	0.002521	91.15%	90.30%
Recovery*	0.003834	0.003136	0.003099	18.20%	19.17%
Sensor drift	0.020719	0.002966	0.002825	88.13%	88.83%
Passthrough	0.020719	0.001095	0.001132	97.00%	96.83%

Table 3: Losses and recovery. \*Lesioned loss and percent recoveries based on the post-recovery values. “Coadapt” refers to co-adaptation. “Con” refers to F5-M1 connection lesions. “Recovery” refers to the experiment involving recovery prior to co-processor training. For further exploration of the results, see Results.